國 立 交 通 大 學

資訊科學與工程研究所

碩 士 論 文

無線正交分頻多工系統中連續波干擾下之

IQ 不平衡效應的分析與評估

The Analysis and Evaluation of I/Q-Mismatch

Estimation with CW Jamming in

Wireless OFDM Systems

研 究 生：洪誠佑

指導教授：許騰尹 教授

中 華 民 國 九 十 八 年 八 月

無線正交分頻多工系統中連續波干擾下之

IQ 不平衡效應的分析與評估

The Analysis and Evaluation of I/Q-Mismatch Estimation with CW Jamming in Wireless OFDM Systems

研 究 生：洪誠佑　　Student：Cheng-Yu Hung

指導教授：許騰尹　　Advisor：Terng-Yin Hsu

國 立 交 通 大 學

資 訊 科 學 與 工 程 研 究 所

碩 士 論 文

A Thesis

Submitted to Institute of Computer Science and Engineering

College of Computer Science

National Chiao Tung University

in partial Fulfillment of the Requirements

for the Degree of

Master

in

Computer Science

August 2009

Hsinchu, Taiwan, Republic of China

中華民國九十八年八月

摘要

OFDM 系統會遭受 IQ 不平衡（I/Q Mismatch）、載波頻率位移（CFO）、取樣時間位移（SCO）以及直流位移（DC offset）等等許多前端的理想效應。而且，由於許多不同系統可免費使用不用執照的頻帶，因此 OFDM 系統也會受到來自於其他系統窄頻訊號的干擾，例如連續波干擾。此篇論文將會提出一些方法去解決 IQ 不平衡（I/Q Mismatch），且是在有連續波干擾情況下。另外，利用影子拒絕率(IRR)來判斷這些方法的效能。此篇論文有兩個主要的貢獻，第一，在有遵循 802.11n 標準下，提出的演算法只需要一次不複雜的計算就可以估計出 IQ 不平衡（I/Q Mismatch）係數。第二，透過影子拒絕率(IRR)進行模擬的時間可以降低很多。當訊號與干擾波比例等於-10dB 時，理論分析以及模擬結果將證明提出的演算法可以改善系統效能。

Abstract

OFDM systems suffer from the front-end non-ideal effects, such as IQ mismatch (IQM), carrier frequency offset (CFO), sampling clock offset (SCO), DC offset. Furthermore, due to unlicensed frequency bands shared by many different systems, OFDM systems are also interfered with narrowband interference, such as continuous wave (CW) jamming. In this paper, some methods on baseband are proposed to solve I/Q mismatch (IQM) under CW jamming in MIMO-OFDM systems. Through image-rejection-ratio (IRR), the efficiency of these methods is judged. There are two main contributions in this paper. First, by following the 802.11n standard, the proposed algorithm only needs one shoot calculation without too complicated computations. Second, the simulation time can be reduced significantly by IRR. A theoretical analysis and simulation results demonstrate the algorithms can improves the performance while signal-to-jamming ratio (SJR) equals to -10 dB.

Acknowledgement

I would like to thank my advisors, Dr. Terng-Yin Hsu for advice, guidance and care. To my dear isIP Lab. members, this work would have been impossible to be done without your support when I need helps for research, courses, or daily lives. Finally, being grateful to my lovely family, your unselfish love encourages me all the time.

Sincerely, Cheng-Yu Hung

August 2009

Table of Contents

摘要 ..... **i**
Abstract ..... **ii**
Acknowledgement ..... **iii**
Table of Contents ..... **iv**
List of Figures ..... **vi**
List of Tables ..... **viii**
Chapter 1 Introduction **1**
Chapter 2 System Platform **6**
2.1 Simulation Platform 6
2.1.1 Transmitter 6
2.1.2 Receiver 8
2.1.3 Channel Model 9
2.1.4 Packet Format 10
2.2 I/Q Mismatch Model 11
2.3 CW Jamming Model 13
Chapter 3 Analysis and Methods **18**
3.1 I/Q Mismatch Estimation in Frequency Domain (FD-IQME) 19
3.2 Analysis of CW Jamming 22
3.2.1 Amplitude, Phase, Power of CW Jamming 23
3.2.2 Ratio of CW Jamming and Preamble Patterns in Aspect of Power 27
3.3 CW Jamming Detection 28
3.4 Anti-Jamming Method 29
3.5 Peak-Avoidance Method (PEAM) 30
3.6 Smooth Filter 31
3.7 Averaging Method in Time Domain (TD-AVM) 32
3.8 The Proposed Algorithm of I/Q Estimation with CW Jamming 34

Chapter 4 Simulation Results and Performance 36
4.1 Simulation Results of Only I/Q-Mismatch 36
4.2 Performance Index 38
4.3 Simulation Results of I/Q-Mismatch with CW Jamming 39
4.3.1 Evaluate FD-IQME 39
4.3.2 Evaluate SF & SP-LP 41
4.3.3 Evaluate PEAM & TD-AVM 42
4.3.4 Brief Summary 44
Chapter 5 Conclusions and Future Work 46
5.1 Conclusions 46
5.2 Future Work 46
5.2.1 I/Q Mismatch Estimation in Time Domain 47
5.2.2 Channel Estimation 47
5.2.3 Hardware Implementation 47
Bibliography 48

List of Figures

Figure 1-1 CW Jamming emits from other electrical equipments. 4
Figure 1-2 The unlicensed band used for ISM and UNII. 4
Figure 2-1 IEEE 802.11n MIMO Transmitter 7
Figure 2-2 Alamouti STBC（Space Time Block Code） 8
Figure 2-3 IEEE 802.11n MIMO Receiver 9
Figure 2-4 Baseband equivalent system model 9
Figure 2-5 IEEE 802.11n Packet Format.....10
Figure 2-6 MIMO-OFDM Receiver I/Q Mismatch System Model. 12
Figure 2-7 16QAM constellation, w/o AWGN, with TGN E.(a)Without I/Q mismatch (b)Gain error: 1dB, Phase error: 10degree. 13
Figure 2-8 CW jamming in Time Domain. (a)CR=133k. (b)CR=667k. 15
Figure 2-9 X axis : frequency , Y axis : # of symbol , Z axis :magnitude. CW jamming in Frequency Domain (3D). 16
Figure 2-10 CW jamming in Frequency Domain (2D). 16
Figure 2-11 16QAM constellation, SNR=25dB, with TGN E. (a)Without CW Jamming. (b)With CW Jamming, SJR=-10dB. 17
Figure 3-1 (a)The real part of preambles in time domain. (b)The real part of CW jamming in time domain. (c)The image part of preambles in time domain. (c)The image part of CW jamming in time domain. 24
Figure 3-2 64 samples taken from preamble and CW jamming. 24
Figure 3-3 Power and phase of preambles and CW jamming in time domain. 25
Figure 3-4 Power and phase of preambles and CW jamming in frequency domain....26
Figure 3-5 Power Distribution on Each Subcarrier Index. 26
Figure 3-6 Power Distribution on 12 Subcarrier Indexes. 28
Figure 3-7 CW Jamming and L-STF in Frequency Domain. 31
Figure 3-8 Smooth Filter block diagram. 32

Figure 3-9 Channel Frequency Response. 32
Figure 3-10 Comparison of power of CW jamming between before and after TD-AVM. 33
Figure 3-11Probability density function (PDF) of power of Subcarrier index 17. (a)Before TD-AVM. (b)After TD-AVM. 34
Figure 3-12 The proposed algorithm structure in Rx. 35
Figure 3-13 The flow chart of the proposed algorithm. 35
Figure 4-1 The Compensation Result. 37
Figure 4-2 IRR values corresponding to different phases and gains. 38
Figure 4-3 IRR, comparison of FD-IQME w/o jamming and FD-IQME with CW jamming. 40
Figure 4-4 IRR, comparison of FD-IQME w/o jamming, FD-IQME with CW jamming, and FD-IQME+SF with jamming. 41
Figure 4-5 IRR, comparison of FD-IQME w/o jamming, FD-IQME with CW jamming, and FD-IQME+SP-LP with jamming. 42
Figure 4-6 Probability density function (PDF) of IRR. (a) FD-IQME. 43
Figure 4-7 IRR, comparison of FD-IQME w/o jamming, FD-IQME with jamming, PEAM+ FD-IQME with jamming, and TD-AVM+PEAM+ FD-IQME with jamming. 45

List of Tables

Table 1-1 The state of the art. 5
Table 4-1 IRR, comparison of FD-IQME w/o jamming and FD-IQME with CW jamming 40
Table 4-2 IRR, comparison of FD-IQME, PEAM+ FD-IQME, and TD-AVM+PEAM+ FD-IQME 44
Table 4-3 IRR, comparison of FD-IQME w/o jamming, FD-IQME with jamming, PEAM+ FD-IQME with jamming, and TD-AVM+PEAM+ FD-IQME with jamming 45

Chapter 1

Introduction

Orthogonal frequency division multiplexing (OFDM) technique, which has been adopted for digital audio broadcasting, digital video broadcasting terrestrial TV and 802.11 series, has become a more and more popular modulation in wireless communications due to its spectrally efficient capability of mitigating the multipath fading channel or inter-symbol interference. The IEEE P802.15.3 wireless person area network (WPAN), the IEEE 802.11a/b/g/n wireless local area network (WLAN), the IEEE 802.16 wireless metropolitan area network (WMAN) and the IEEE 802.20 mobile broadband wireless access (MBWA) choose this technique due to providing high data rate. However, OFDM systems are highly susceptible to the non-ideal front-end effects, which are caused by the imperfections of analog electric components. Due to fabrication process variations, these effects, which are unpredictable and uncontrollable, often occur in the analog electric components. A major origin of non-ideal front-end effects in front-end wireless system is In-phase and Quadrature-phase mismatch (IQM). In other words, the I/Q mismatch is a difference between I and Q branches form ideal case, which is denoted by not exact 90^0 phases and unequal gain. Furthermore, narrowband interference, which significantly degrades system performance, can be discovered in wireless channels

such as continuous-wave (CW) jamming, as can be seen from Figure 1-1. Narrowband interference is denoted as a signal whose occupied frequency bandwidth is smaller than others. The unlicensed band is a free frequency bandwidth which each system can use, as can be seen from Figure 1-2. So the unlicensed band is shared by various systems such as Bluetooth, microwave, and 802.11 series whose signals interfere with each other and are referred to as narrowband interference. For instance, WiMAX is a narrowband interferer for UWB systems. If the spectrum of an OFDM was overlapped by other system signals, OFDM system performance will suffer from serious degradation.

In the literature, there are many methods proposed for the compensation of I/Q mismatch. Some methods of estimating I/Q mismatch were provided by designing the OFDM training symbols [1]. Based on the assumption that desired signal and image interference are statistically independent, some methods make use of the blind source separation techniques to extract the desired signal [2] [3] [4] [5]. The correction method discussed in [6] can only compensate the IQM with gain error up to 0.414dB and phase error to 10 degree, which does not reach the conventional tolerance, saying gain error 1 dB and phase error 10 degree. Another approach is to do the work by analog circuit [7]. There has been a great deal of research concerning mitigation of jamming in an OFDM system. Some of the techniques range include from using orthogonal codes [8]–[10], frequency-domain cancellation [11], [12], receiver windowing [13], and excision filtering [14]. Table 1-1 shows the state of the art of IQM and CW jamming separately. However, there are few papers providing the methods of jointly considering IQM and CW jamming.

In this work, an MIMO-OFDM system is chosen in the presence of AWGN, multipath fading channel, IQM, and CW jamming. In addition, most researchers assumed the source of CW jamming was close to the receiver and went through no multipath fading channels. However, it is more reasonable and practical to assume

that the jamming signal experiences another separate channel. Because of in most cases, the sources of the jamming are emitted from remote areas such as satellites in the space or battleships at the sea. Even if the sources of the jamming come from some systems indoors, the jamming signal also experiences separate channels. Specifically, we focus on the investigation of the jamming and consider jointly the effects of IQM and CW jamming. Simple frequency domain anti-jamming techniques are examined for MIMO-OFDM systems, i.e., peak-avoidance method. Some methods of estimating IQM correctly under CW jamming will be proposed, and a series of analysis will be presented through simulation results. The main contribution for this paper is as follows. First, following the 802.11n standard, one of the proposed algorithms only needs one shot calculation to estimate IQM without too complicated methods. Second, by defining image-rejection-ratio (IRR), the simulation time can be effectively reduced. The proposed algorithm demonstrates that the performance of MIMO-OFDM systems is better through image-rejection-ratio (IRR).

This paper is organized as follows: Chapter 2 describes the system model in detail. Chapter 3 presents an overview of the anti-jamming method and I/Q mismatch estimation employed in MIMO-OFDM systems; performance results are illustrated in Chapter 4. Conclusions and future work are presented in Chapter 5.

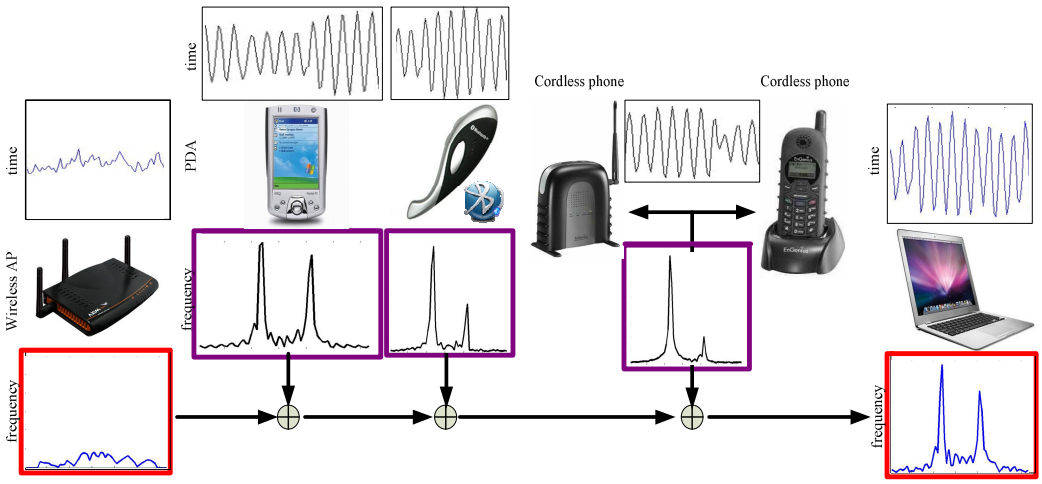

Figure 1-1 CW Jamming emits from other electrical equipments.

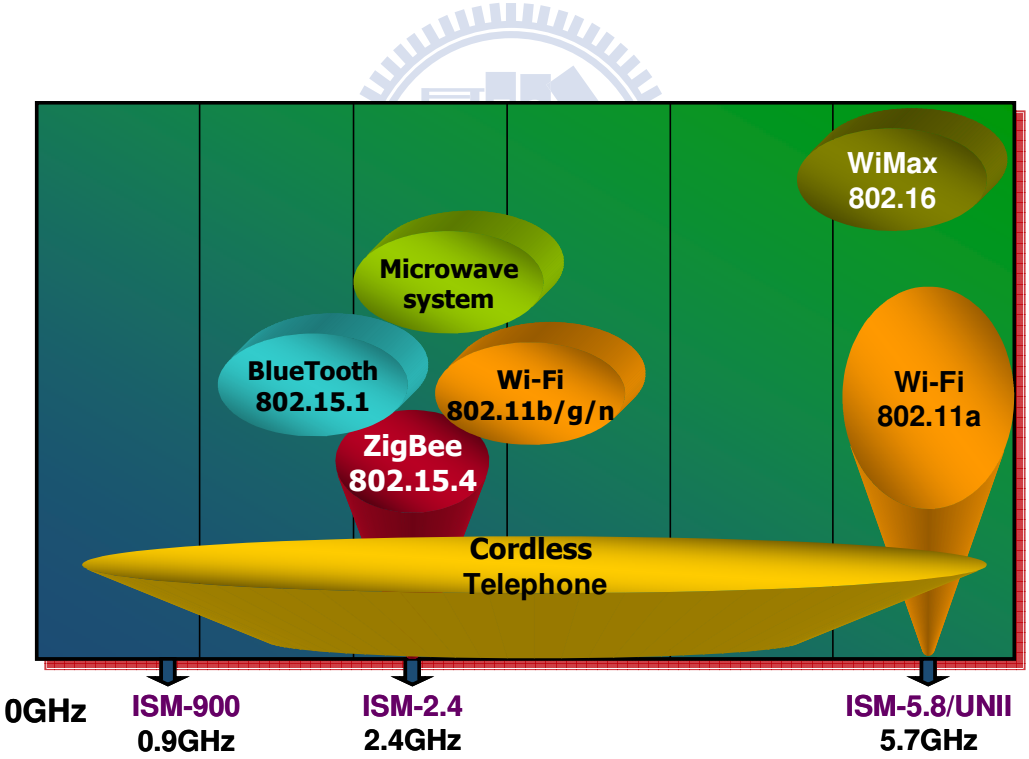

Figure 1-2 The unlicensed band used for ISM and UNII.

Table 1-1 The state of the art.

class	*Ref.*	*Description*	*Note*
IQM	**[4]**	**Blind source seperation**	**Convergence condition is not guaranteed.**
	[6]	**Joint estimation of I/Q-M & CFO**	**I/Q Mismatch tolerance does not reach the general requirements.**
CW Jamming	**[8]**	**Orthogonal codes for resisting jamming**	**The cost of orthogonal codes is needed.**
	[11]	**LMMSE canceller for narrowband interference**	**1. It needs more data symbols to reduce jamming effect.** **2. The matrix of Computational complexity is high due to many matrix operations.**

Chapter 2

System Platform

MIMO-OFDM systems operate at 2.4GHz band with 20MHz bandwidth, which follows MIMO-OFDM specification of IEEE 802.11n PHY layer of the TGn Sync Proposal. Section 2.1 describes the MIMO transceivers, channel models and the packet format of 802.11n. I/Q mismatch model and CW jamming model are introduced in section 2.2 and section 2.3, respectively.

2.1 Simulation Platform

The simulation platform is MIMO-OFDM system, which is built according to the standard of IEEE. 802.11n. Three main blocks are in this platform, including transmitter, channel model, and receiver. The MIMO-OFDM system operates in 20 MHz and can transmit data by 2x2 or 4x4 antennas. Each OFDM symbol is constructed from 56 tones, of which 52 are data tones and 4 are pilot tones. The tone mapping is identical to that in IEEE 802.11a [15] (subclause 17.3.5.9 in reference) except the 2 extra tones on either side.

2.1.1 Transmitter

The transmitter block diagram of MIMO-OFDM specified in IEEE 802.11n proposal is shown as Figure 2-1. The source data is first scrambled to prevent a

succession of zeros or ones, and then it is encoded by convolution encoder, which is used as Forward Error Correction (FEC). The FEC-encoded bit stream is punctured in order to support four coding rates, 1/2, 2/3, 3/4 and 5/6. Then the punctured bit stream is parsed into spatial streams, according to the number of transmit antennas.

To prevent burst error, the interleaver is used to change the order of bits for each spatial stream. Then the interleaved sequence of bit in each spatial stream is modulated (to complex constellation points), there are four kinds of modulations, BPSK, QPSK, 16-QAM and 64-QAM. The STBC (Space Time Block Code) encoder, which is shown in Figure 2-2, spreads the constellation points of each spatial stream to any other spatial streams.

To transform the STBC-encoded frequency domain constellations into time-domain constellations, Inverse Fast Fourier Transform (IFFT) is used. There are 64 frequency entries for each IFFT, or 64 sub-carriers in each OFDM symbol. 52 of them are data carriers, 4 of them are pilot carriers and the rest 8 are null carriers. Finally, the time domain signals appended to the Guard Interval (GI) of 1/4 symbol length, are transmitted by RF modules.

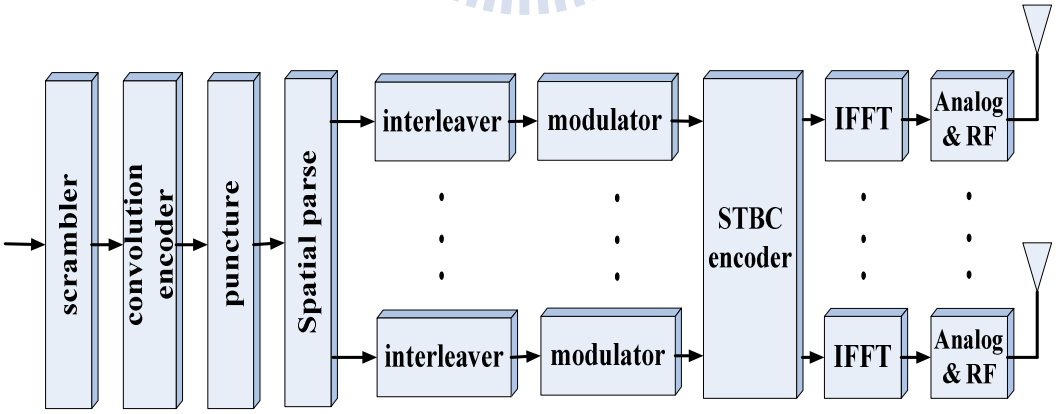

Figure 2-1 IEEE 802.11n MIMO Transmitter

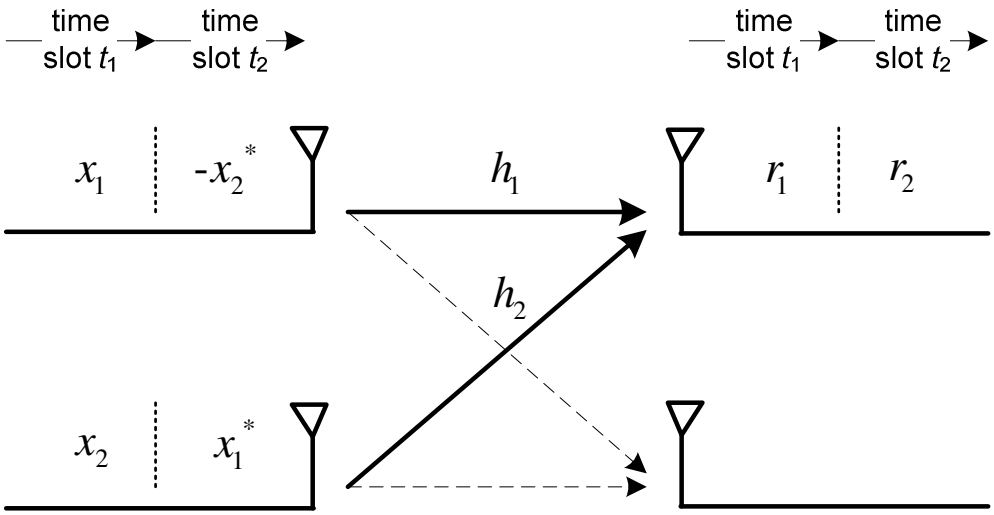

Figure 2-2 Alamouti STBC（Space Time Block Code）

2.1.2 Receiver

The receiver block diagram of MIMO-OFDM specified in IEEE 802.11n proposal is shown as Figure 2-3. Signals received from the RF modules are first synchronized to recognize each OFDM symbol. Each OFDM symbol is transformed to frequency domain by the Fast Fourier Transform (FFT). If the OFDM symbol belongs to long preamble (described in section 2.1.3), then it is used for channel estimation [16]. Otherwise, it belongs to payload and is decoded by STBC decoder, which needs the CFR information estimated by the channel estimation block. The STBC decoder can be seen as the equalizer of MIMO-OFDM systems and it is introduced in section 2.1.1.

After separated by STBC decoder, the spatial streams are demodulated to bit-level streams. Then these bit-level data streams are de-interleaved and merge to single data stream. Finally, the data stream is decoded by FEC which includes de-puncturing, Viterbi decoder and de-scrambler.

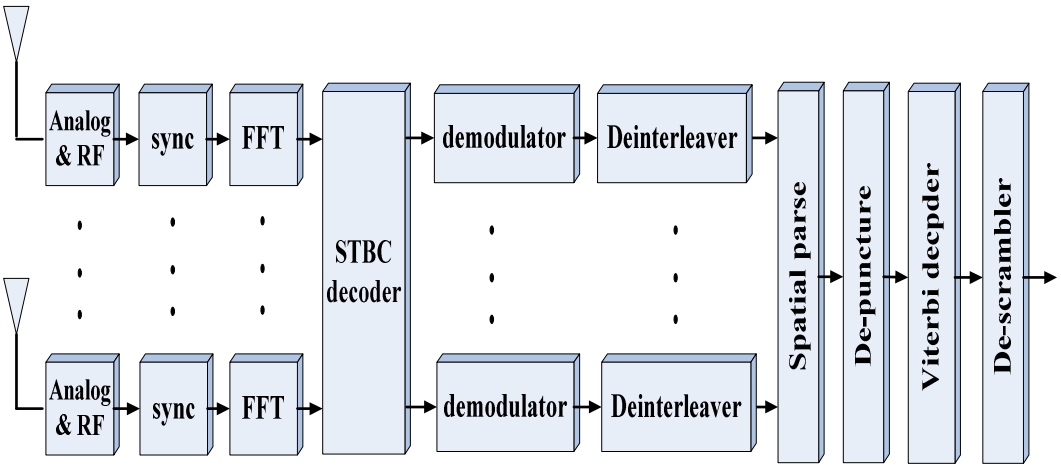

Figure 2-3 IEEE 802.11n MIMO Receiver

2.1.3 Channel Model

AWGN, multipath fading channel, I/Q mismatch, and CW jamming are simulated in the channel. The AWGN is added, the multipath fading channel is convoluted, IQ mismatch is multiplied and CW jamming is added to the Tx signal. The parameter of the AWGN channel is the signal-to-noise ratio (SNR) in dB; the parameter of the CW jamming is the signal-to-jamming ratio (SJR) in dB. IQM will introduce two parameters, i.e. gain error and phase error. As for the multipath fading channel, the parameters include the channel types, the root-mean-square (rms) delay spread value and the tap numbers. Figure 2-4 shows the practical and the baseband equivalent channel model.

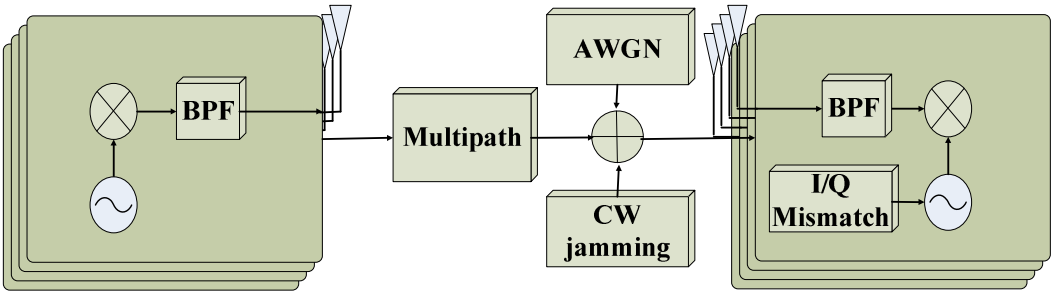

Figure 2-4 Baseband equivalent system model

2.1.4 Packet Format

The packet format fields are shown as Figure 2-5. The L-STF (Legacy Short Training Field), the L-LTF (Legacy Long Training Field), L-SIG (Legacy Signal Field) and HT-SIG (High Throughput Signal Field) comprise the legacy compatible part of the PPDU preamble which allows PHY layer interoperability with 802.11a and ERP-802.11g modems.

The HT-STF fields stands for High-Throughput Short Training Field, and it is short preamble of MIMO-OFDM systems which is used for synchronizing to recognize each OFDM symbol. The HT-LTF fields stand for High-Throughput Long Training Field, that is, the long preambles for MIMO-OFDM systems. The long preambles are used for channel estimation as described in [16]. The payload parts shown as DATA fields in Figure 2-6, each symbol consisting of 52 data sub-carriers and 4 pilot sub-carriers, are used for the adaptive channel estimation algorithm [17].

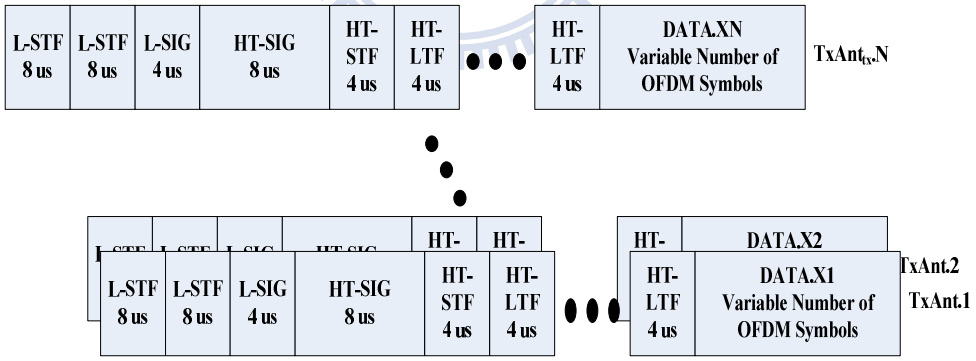

Figure 2-5 IEEE 802.11n Packet Format

2.2 I/Q Mismatch Model

I/Q mismatch caused by the LO can be introduced by a gain error g = (1+ε) and a phase error θ. Followed the LO, different mixers, amplifiers, LPFs and A/D converters used in both In-phase and Quadrature-phase paths cause the frequency dependent I/Q imbalance. But in this paper, the frequency independent I/Q mismatch is assumed. A block-diagram of an I/Q signal processing based MIMO-OFDM receiver is shown in Fig.2-6.

The effect of quadrature demodulator: The local oscillator signal $X_{LO}(t)$ of an imbalanced quadrature demodulator is here modelled as [18]:

$$\begin{aligned} X_{LO}(t) &= I_{LO}(t) + jQ_{LO}(t) \\ &= 2\cos(2\pi f_c t) - 2jg\sin(2\pi f_c t + \theta) \\ &= 2K_1 e^{-j2\pi f_c t} + 2K_2 e^{j2\pi f_c t} \\ &= 2K_1 z(t) + 2K_2 z^*(t), \end{aligned} \tag{1}$$

where g = (1+ε) and θ represent the demodulator gain and phase error, respectively (ideally g = 1 and θ = 0). The mismatch coefficients K_1 and K_2 in (1) are given by

$$K_1 = [1 + ge^{-j\theta}]. \tag{2a}$$

$$K_2 = [1 - ge^{j\theta}]. \tag{2b}$$

The transmitted signal $x(t) = x_I(t) + jx_Q(t)$ will multiply with carrier frequency f_c and then be sent by RF in the transmitter. Therefore, the baseband equivalent signal received from RF in the receiver can be expressed as

$$z(t) = x_I(t)\cos(2\pi f_c t) - x_Q(t)\sin(2\pi f_c t). \tag{3}$$

To analyze the effect of I/Q mismatch, after the received signal goes through mixers, LPF, and ADC, it can be rewritten as

$$\begin{aligned} r(n) &= I(n) + jQ(n) \\ &= \alpha x(n) + \beta x^*(n). \end{aligned} \tag{4}$$

where

$\alpha = [1 + ge^{-j\theta}]/2$.

$\beta = [1 - ge^{j\theta}]/2$.

These two parameters, α and β are called IQM coefficient. In OFDM system, the signal $r(t)$ is transformed into frequency domain by Fast-Fourier Transform (FFT).

$$\begin{aligned} R(k) &= FFT\{I(n) + jQ(n)\} \\ &= \alpha X(k) + \beta X^*(-k). \end{aligned} \tag{5}$$

In (4), the term $x^*(n)$ is named the image signal caused by I/Q mismatch because it appears at the corresponding negative frequency position to interfere with the original signal. Here, n presents sampling index; k presents subcarrier index. Notice that the basic mismatch model used in [19]-[20] is the case of (5). The image signal cannot be attenuated mostly in the front-end processing. Without some kind of compensation for I/Q mismatch, the system degrades sufficiently. Figure 2-7 shows the effect of I/Q mismatch on OFDM systems.

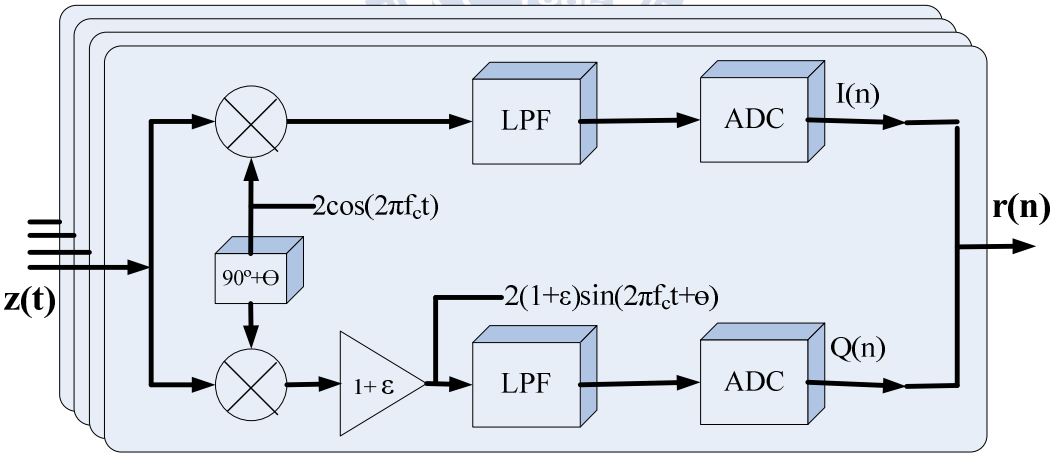

Figure 2-6 MIMO-OFDM Receiver I/Q Mismatch System Model.

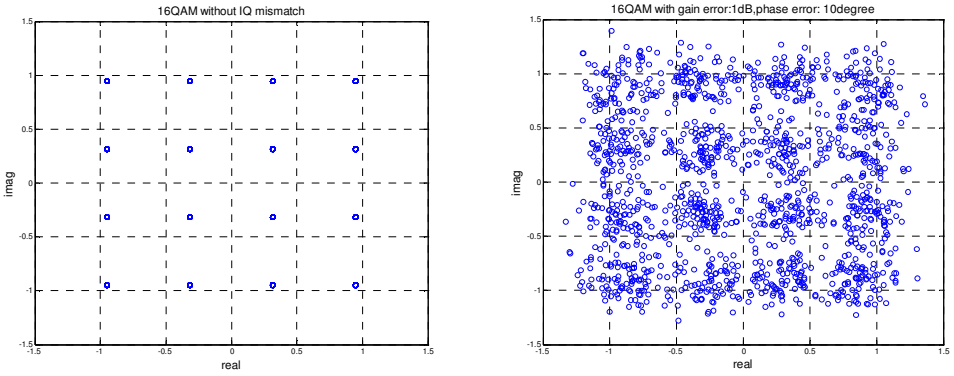

(a) (b)

Figure 2-7 16QAM constellation, w/o AWGN, with TGN E.(a)Without I/Q mismatch (b)Gain error: 1dB, Phase error: 10degree.

2.3 CW Jamming Model

When signals $s(t)$ are transferred from transmitters through channels, they are interfered by white Gaussian noise $n(t)$. Furthermore, before receivers receive signals, they are interfered by other intentional or an unintentional CW jamming $i(t)$ which experiences a fading channel $h_j(t)$, the received signals are expressed as the following:

$$r(t) = s(t) + n(t) + i(t) \otimes h_j(t). \quad (6)$$

where the symbol $\otimes$ represents convolution.

When jammers are delivered by a stable carrier, they are called as continuous-wave (CW) jamming. The jamming has their own changing rate (CR) which is denoted as how long transmitted data bit changes per second. Generally speaking, if the ratio of changing rate and system bandwidth is not greater than $1/30$, CW jamming is called as narrowband interference. Changing rate will decide amplitude rate (AR) which is defined as how long the magnitude of the jamming will change its value and keep its value for a period of time. Changing rate also decides phase rate (PR) which is defined as how long the phase offset of the jamming will

change its value and keep its value for a period of time. Depending on different values of amplitude rate and phase rate will directly the amplitude and the phase of the jamming in the time domain and indirectly change the waveform of the jamming in the frequency domain which makes their fractional power containment bandwidth adopted by FCC become rougher and interfere with more subcarriers of MIMO-OFDM systems.

In this paper, both single-tone continuous-wave jamming and multi-tone continuous-wave jamming with QPSK modulation are introduced.

1. Single-Tone Continuous-Wave Jamming

The mathematical equation is expressed as

$$i(t) = A \cdot \cos(2\pi ft + \theta_I) + B \cdot j\sin(2\pi ft + \theta_Q), \tag{7}$$

where A 、 B represent the amplitude of in-phase and quadrature-phase path of a jammer, f represents the carrier frequency of a jammer, θ_I, θ_Q represent the phase offset of in-phase and quadrature-phase path of a jammer respectively.

2. Multi-Tone Continuous-Wave Jamming

The mathematical equation is expressed as

$$i(t) = \sum_{n=1}^{N}\left[A_n \cdot \cos(2\pi f_n t + \theta_{I,n}) + B_n \cdot j\sin(2\pi f_n t + \theta_{Q,n}) \right], \tag{8}$$

where A_n 、 B_n represent the amplitude of in-phase and quadrature-phase path of the nth jammer, f_n represents the carrier frequency of the nth jammer, $\theta_{I,n}, \theta_{Q,n}$ represent the nth phase offset of in-phase and quadrature-phase path of the nth jammer.

For single-tone continuous-wave jamming and multi-tone continuous-wave jamming, parameters of them, frequency, amplitude and phase, satisfy with the following below:

random frequency : $0MHz \le f_c \le 20MHz$.

random amplitude : $A^2 + B^2 = 1$.

random phase : $-10° \le \theta_I, \theta_Q \le 10°$.

Figure 2-8 presents that CW jamming changes in time domain according to different changing rates (CR).

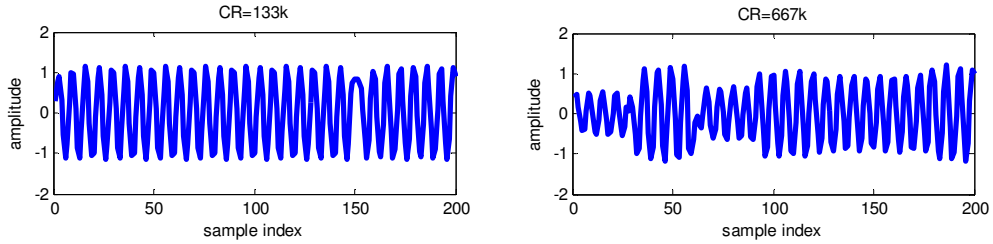

(a) (b)

Figure 2-8 CW jamming in Time Domain. (a)CR=133k. (b)CR=667k.

Figure 2-9 shows that MATLAB is used to simulate single-tone continuous-wave Jamming. It illustrates that the change of main lobe of the jamming in frequency domain depends on the condition of amplitude rate and phase rate. The main bandwidth occupied by the main power of CW jamming is about the quarter of 20 MHz. For 20MHz OFDM systems, CW jamming is narrowband interference.

The simulation environment is the following: Modulation：4X4, 64QAM, signal to jamming ratio (SJR)：-10 dB, CW tone number：1, changing rate：33k bps. Figure 2-10 represents the 2D floor plan of the first, fifth and thirty-five symbols of Figure 2-9 and it clearly shows that the bandwidth range occupied by their main lobes are different. Figure 2-11 shows the effect of CW jamming on OFDM systems.

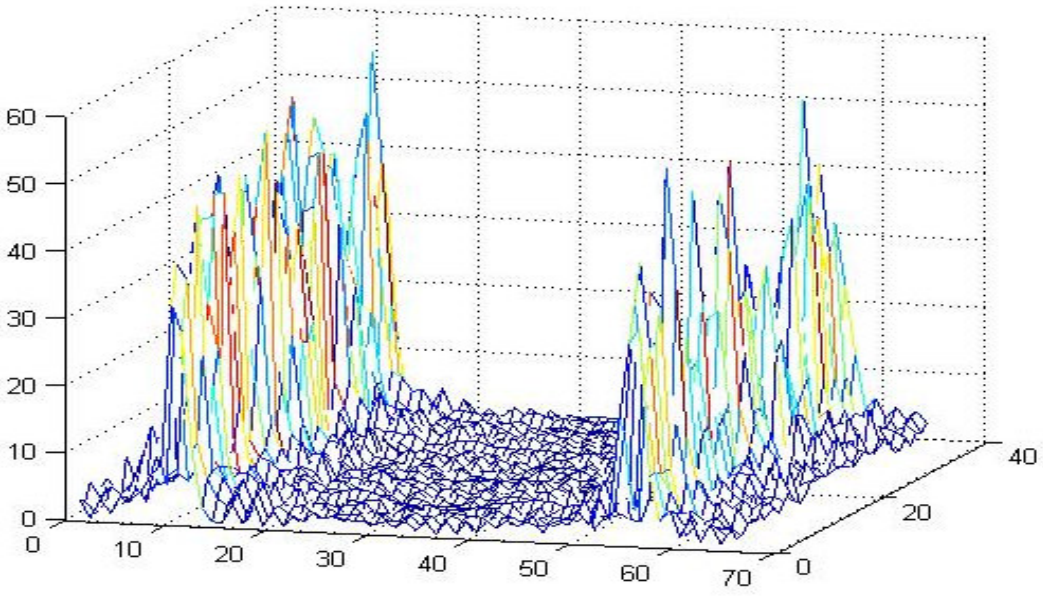

Figure 2-9 X axis : frequency , Y axis : # of symbol , Z axis :magnitude. CW jamming in Frequency Domain (3D).

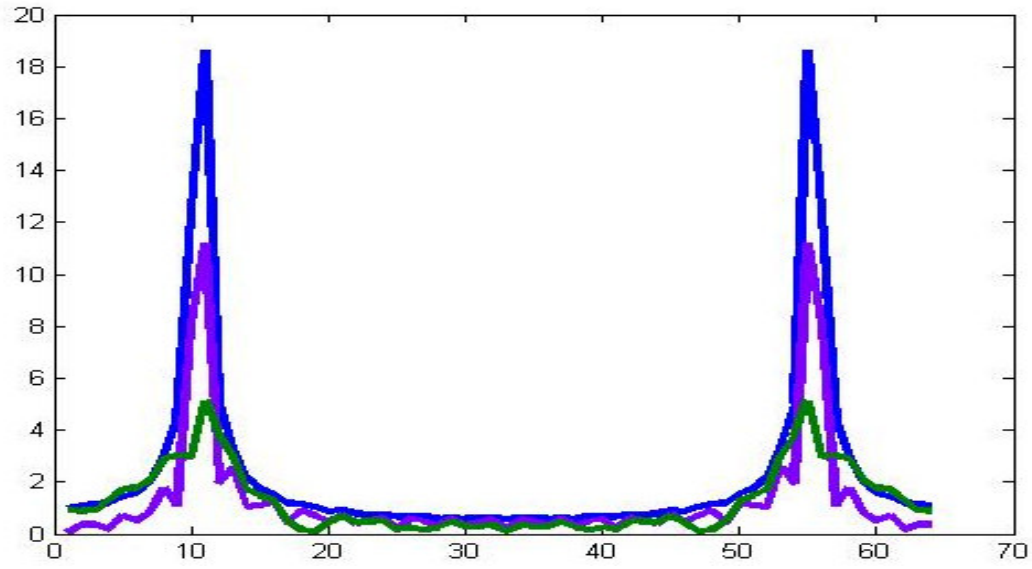

Figure 2-10 CW jamming in Frequency Domain (2D).

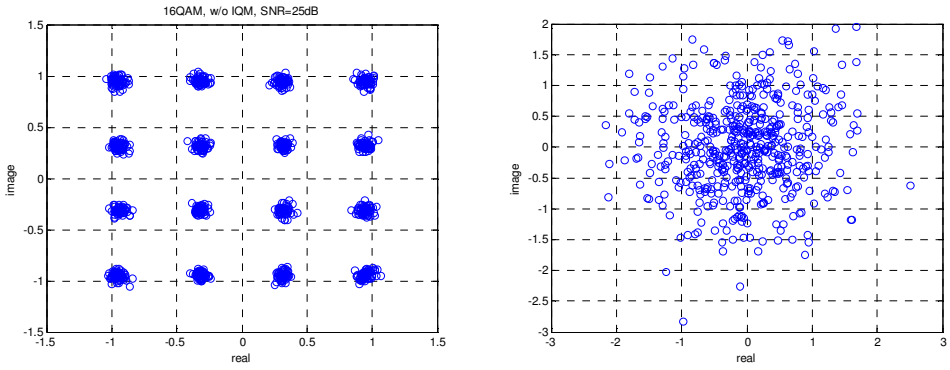

(a) (b)

Figure 2-11 16QAM constellation, SNR=25dB, with TGN E. (a)Without CW Jamming. (b)With CW Jamming, SJR=-10dB.

Chapter 3

Analysis and Methods

In this chapter, FD-IQME is proposed to solve I/Q mismatch by using short preamble based on the IEEE 802.11n standard. Then, some analysis for CW jamming form different aspects are presented; some methods for IQM under CW jamming are suggested.

Section 3.1 describes I/Q mismatch estimation in frequency domain. CW jamming will be analyzed from different aspects, including the amplitude, phase, power, and the ratio between CW jamming and preamble patterns in section 3.2. CW jamming detection is described in section 3.3. In section 3.4, one anti-jamming method is suggested to solve I/Q mismatch and CW jamming under some assumptions, but it is impractical enough. Peak-Avoidance Method (PEAM) and Averaging Method in Time Domain (TD-AVM) are introduces in section 3.5 and section 3.7; a smooth filter is proposed for getting accurate CFR in section 3.6. Finally, the Proposed Algorithm of I/Q Estimation with CW Jamming is depicted step by step in section 3.8.

3.1 I/Q Mismatch Estimation in Frequency Domain (FD-IQME)

In MIMO-OFDM system, the packet format based on the IEEE 802.11n is shown as Figure 2-5. The legacy short training (L-STF) and legacy long training OFDM symbol (L-LTF) are identical to the 802.11a short training and long training OFDM symbol. The high-throughput long training OFDM symbols (HT-LTF) are transmitted after one high-throughput short training OFDM symbol (HT-STF). For any PPDU, the number of HT-LTF is the same as spatial streams in the HT Data portion of the PPDU. Each HT-LTF consists of one legacy Long Training Symbols (LTS) of 3.2 μs as in 802.11a/g and a regular guard interval of 0.8 μs, giving a total length of 4μs. The cyclic shift (CSD) is applied to each OFDM symbol. Therefore, the L-STF, the L-LTF, the HT-STF and the HT-LTF are shifted according to different cyclic shift values of each antenna in time domain.

By making use of the received HT-LTF, the channel frequency response can be roughly estimated. Taking 2x2 system for example, these channel frequency responses $\hat{H}_{RT}(f)$, which means the estimating channel frequency response of Tth transmitter antenna to Rth receiver antenna, can be obtained as follows:

$$\hat{H}_{11}(k) = \alpha_1 H_{11}(k) + \beta_1 H_{11}^*(-k) \frac{HT\text{-}LTF_1^*(-k)}{HT\text{-}LTF_1(k)}. \quad (9)$$

$$\hat{H}_{12}(k) = \alpha_1 H_{12}(k) + \beta_1 H_{12}^*(-k) \frac{HT\text{-}LTF_1^*(-k)}{HT\text{-}LTF_1(k)}. \quad (10)$$

$$\hat{H}_{21}(k) = \alpha_2 H_{21}(k) + \beta_2 H_{21}^*(-k) \frac{HT\text{-}LTF_2^*(-k)}{HT\text{-}LTF_2(k)}. \quad (11)$$

$$\hat{H}_{22}(k) = \alpha_2 H_{22}(k) + \beta_2 H_{22}^*(-k) \frac{HT\text{-}LTF_2^*(-k)}{HT\text{-}LTF_2(k)}. \quad (12)$$

where α_N and β_N mean the IQM coefficients in receiver N, and $H_{RT}(k)$ represent the real channel frequency responses; $L\text{-}LTF(k)$ represent the ideal pattern of legacy long preambles. Because the ideal pattern of L-STF and L-LTF are known,

the values $\frac{L\text{-}STF^{*}(-k)}{L\text{-}STF(k)}$ 、$\frac{HT\text{-}LTF^{*}(-k)}{HT\text{-}LTF(k)}$ can be calculated first on each frequency position. If the term $\frac{L\text{-}STF^{*}(-k)}{L\text{-}STF(k)}$ is divided by the term $\frac{HT\text{-}LTF^{*}(-k)}{HT\text{-}LTF(k)}$, the quotient $\frac{L\text{-}STF^{*}(-k)}{L\text{-}STF(k)} \Big/ \frac{HT\text{-}LTF^{*}(-k)}{HT\text{-}LTF(k)}$ will be j or $-j$.

The received L-STF in receiver one is expressed as

$$\begin{aligned} R_1(k) &= \alpha_1 L\text{-}STF_1(k)H_{11}(k) + \beta_1 L\text{-}STF_1^{*}(-k)H^{*}{}_{11}(-k) \\ &\quad + \alpha_1 L\text{-}STF_2(k)H_{12}(k) + \beta_1 L\text{-}STF_2^{*}(-k)H^{*}{}_{12}(-k). \end{aligned} \tag{13}$$

Equation (13) can be rewritten as

$$\begin{aligned} R_1(k) &= L\text{-}STF_1(k)[\alpha_1 H_{11}(k) + \beta_1 \frac{L\text{-}STF_1^{*}(-k)}{L\text{-}STF_1(k)} H^{*}{}_{11}(-k)] \\ &\quad + L\text{-}STF_2(k)[\alpha_1 H_{12}(k) + \beta_1 \frac{L\text{-}STF_2^{*}(-k)}{L\text{-}STF_2(k)} H^{*}{}_{12}(-k)]. \end{aligned} \tag{14}$$

If the quotient $\frac{L\text{-}STF^{*}(-k)}{L\text{-}STF(k)} \Big/ \frac{HT\text{-}LTF^{*}(-k)}{HT\text{-}LTF(k)}$ is equal to j and equation (9) and (10) are used, equation (14) can be rewritten as

$$\begin{aligned} R_1(k) &= L\text{-}STF_1(k)[j\hat{H}_{11}(k) - \alpha_1 jH_{11}(k) + \alpha_1 H_{11}(k)] \\ &\quad + L\text{-}STF_2(k)[j\hat{H}_{12}(k) - \alpha_1 jH_{12}(k) + \alpha_1 H_{12}(k)]. \end{aligned} \tag{15}$$

After some rearrangement and making the new equation conjugate, equation (15) can be derived as

$$\begin{aligned} &\alpha_1^{*}(1+j)[L\text{-}STF_1^{*}(-k)H_{11}^{*}(-k) + L\text{-}STF_2^{*}(-k)H_{12}^{*}(-k)] = \\ &R_1^{*}(-k) + L\text{-}STF_1^{*}(-k)\,jH_{11}^{*}(-k) + L\text{-}STF_2^{*}(-k)\,jH_{12}^{*}(-k). \end{aligned} \tag{16}$$

By the same method, equation (14) can be rewritten another form as follows:

$$\begin{aligned} R_1(k) &= L\text{-}STF_1(k)[\hat{H}_{11}(k) + \beta_1 H^{*}{}_{11}(-k) \frac{HT\text{-}LTF_1^{*}(-k)}{HT\text{-}LTF_1(k)}(-1+j)] \\ &\quad + L\text{-}STF_2(k)[\hat{H}_{12}(k) + \beta_1 H^{*}{}_{12}(-k) \frac{HT\text{-}LTF_1^{*}(-k)}{HT\text{-}LTF_1(k)}(-1+j)]. \end{aligned} \tag{17}$$

After some rearrangement and making the new equation conjugate, equation (17) can be derived as

$$\beta_1(1-j)\frac{HT\text{-}LTF_1^*(-k)}{HT\text{-}LTF_1(k)}[L\text{-}STF_2(k)H_{11}^*(-k)+L\text{-}STF_2(k)H_{12}^*(-k)]= \\ -R_1(k)+L\text{-}STF_1(k)\hat{H}_{11}(k)+L\text{-}STF_2(k)\hat{H}_{12}(k). \tag{18}$$

Let equation (18) be divided by equation (16) and then rearrange the equation. An estimated IQM coefficient will be obtained as follows:

$$\frac{\beta_1}{\alpha_1^*}=\frac{R_1(k)-L\text{-}STF_1(k)\hat{H}_{11}(k)-L\text{-}STF_2(k)\hat{H}_{12}(k)}{R_1^*(-k)-L\text{-}STF_1(k)\hat{H}_{11}^*(-k)QHT-L\text{-}STF_2(k)\hat{H}_{12}^*(-k)QHT}. \tag{19}$$

where $QHT=\frac{HT\text{-}LTF_1^*(-k)}{HT\text{-}LTF_1(k)}$.

By following the same steps, if the quotient $\frac{L\text{-}STF^*(-k)}{L\text{-}STF(k)}\Big/\frac{HT\text{-}LTF^*(-k)}{HT\text{-}LTF(k)}$ is equal to and equation (9) and (10) are used, equation (14) can be rewritten as

$$R_1(k)=L\text{-}STF_1(k)[-j\hat{H}_{11}(k)+\alpha_1 jH_{11}(k)+\alpha_1 H_{11}(k)] \\ +L\text{-}STF_2(k)[-j\hat{H}_{12}(k)+\alpha_1 jH_{12}(k)+\alpha_1 H_{12}(k)]. \tag{20}$$

After some rearrangement and making the new equation conjugate, equation (20) can be derived as

$$\alpha_1^*(1-j)[L\text{-}STF_1^*(-k)H_{11}^*(-k)+L\text{-}STF_2^*(-k)H_{12}^*(-k)]= \\ R_1^*(-k)-L\text{-}STF_1^*(-k)\,jH_{11}^*(-k)-L\text{-}STF_2^*(-k)\,jH_{12}^*(-k). \tag{21}$$

By the same method, equation (14) can be rewritten another form as follows:

$$R_1(k)=L\text{-}STF_1(k)[\hat{H}_{11}(k)-\beta_1 H^*{}_{11}(-k)\frac{HT\text{-}LTF_1^*(-k)}{HT\text{-}LTF_1(k)}(1+j)] \\ +L\text{-}STF_2(k)[\hat{H}_{12}(k)-\beta_1 H^*{}_{12}(-k)\frac{HT\text{-}LTF_1^*(-k)}{HT\text{-}LTF_1(k)}(1+j)]. \tag{22}$$

After some rearrangement and making the new equation conjugate, equation (22) can be derived as

$$\beta_1(1+j)\frac{HT\text{-}LTF_1^*(-k)}{HT\text{-}LTF_1(k)}[L\text{-}STF_2(k)H_{11}^*(-k)+L\text{-}STF_2(k)H_{12}^*(-k)]= \\ -R_1(k)+L\text{-}STF_1(k)\hat{H}_{11}(k)+L\text{-}STF_2(k)\hat{H}_{12}(k). \tag{23}$$

Let equation (23) be divided by equation (21) and then rearrange the equation. An estimated IQM coefficient will be obtained as follows:

$$\frac{\beta_1}{\alpha_1^*} = \frac{R_1(k) - L\text{-}STF_1(k)\hat{H}_{11}(k) - L\text{-}STF_2(k)\hat{H}_{12}(k)}{R_1^*(-k) - L\text{-}STF_1(k)\hat{H}_{11}^*(-k)QHT - L\text{-}STF_2(k)\hat{H}_{12}^*(-k)QHT}. \quad (24)$$

where $QHT = \frac{HT\text{-}LTF_1^*(-k)}{HT\text{-}LTF_1(k)}$.

Compared equation (19) with equation (24), whether the quotient $\frac{L\text{-}STF^*(-k)}{L\text{-}STF(k)} \Big/ \frac{HT\text{-}LTF^*(-k)}{HT\text{-}LTF(k)}$ is j or $-j$, the computed result of both is the same.

Based on legacy short training OFDM symbol, there are 12 ratios of $\frac{\beta_1}{\alpha_1^*}$ in the receiver one in MIMO-OFDM 2x2 systems. By averaging the 12 ratios, a final ratio of IQM coefficient will be determined for compensating data distorted by I/Q mismatch. Thus, the IQM coefficient is solved from the equation below.

$$\begin{cases} \frac{\beta_1}{\alpha_1^*} = \frac{R_1(k) - L\text{-}STF_1(k)\hat{H}_{11}(k) - L\text{-}STF_2(k)\hat{H}_{12}(k)}{R_1^*(-k) - L\text{-}STF_1(k)\hat{H}_{11}^*(-k)QHT - L\text{-}STF_2(k)\hat{H}_{12}^*(-k)QHT} \\ \alpha_1^* + \beta_1 = 1 \end{cases} \quad (25)$$

The data of receiver one in frequency domain are compensated by the following equation.

$$\frac{\alpha_1^* R_1(k) - \beta_1 R_1^*(-k)}{\alpha_1 \alpha_1^* - \beta_1 \beta_1^*} \quad (26)$$

In the Receiver two, the same methods are also taken to obtain the 12 ratios of $\frac{\beta_2}{\alpha_2^*}$ to compensate for the frequency dependent I/Q mismatch in receiver two. Above equation from (9) to (26) is the case of 2x2 MIMO-OFDM systems in 20 MHz, these methods can also be applied to solve I/Q mismatch in MIMO-OFDM 4x4 systems.

3.2 Analysis of CW Jamming

In this section, CW jamming will be analyzed from different aspects, including the amplitude, phase, power. The ratio of the transmitted signal and CW jamming is presented latter. The analysis of CW jamming is based on different SJR and changing rate.

3.2.1 Amplitude, Phase, Power of CW Jamming

SJR=-10dB and changing rate= 33kbps is assumed. In time domain, the amplitude of sampled CW jamming varies according to changing rate. Compared CW jamming with preamble patterns (STF/LTF), the amplitude of CW jamming is much larger than the amplitude of preamble patterns due to SJR=-10dB, as can be seen from Figure 3-1. If only 64 sample of CW jamming are taken to observe, the CW jamming almost covers the transmitted signal, as can be seen from Figure 3-2. Figure 3-3 shows that power of CW jamming completely dominate OFDM systems and phase of CW jamming changes randomly. However, something interesting can be found after CW jamming is transferred from time domain into frequency domain by FFT. When one symbol (80 samples) gets rid of cyclic prefix (16 samples) first and then the remainder are taken into FFT, the frequency spectrum of the remainder shows two high peaks at the symmetric subcarrier index. The position of subcarrier index, which is far away from peaks, suffers from less attack of CW jamming. These subcarrier indexes can be used to estimate IQM coefficients. By the same way, the phase of the transmitted signal and CW jamming is shown as figure 3-4. The variation of phase of CW jamming is uncontrollable and unpredictable. Once CW jamming is added to the transmitted signal, the phase of the transmitted signal is hard to recover, not only in time domain but also in frequency domain. The same phenomenon can be discovered from the power of view.

Although the position of subcarrier index far away peaks may be useful to estimate IQM coefficients, the condition is actually more complicated because CW jamming is time-variant for OFDM systems. Different SJR are analyzed here and 1000 packets are used to get a statistics. On different SJR, the power distribution of CW jamming and the transmitted signal are shown as figure 3-5. When SJR decreases, the power on each subcarrier index will increase.

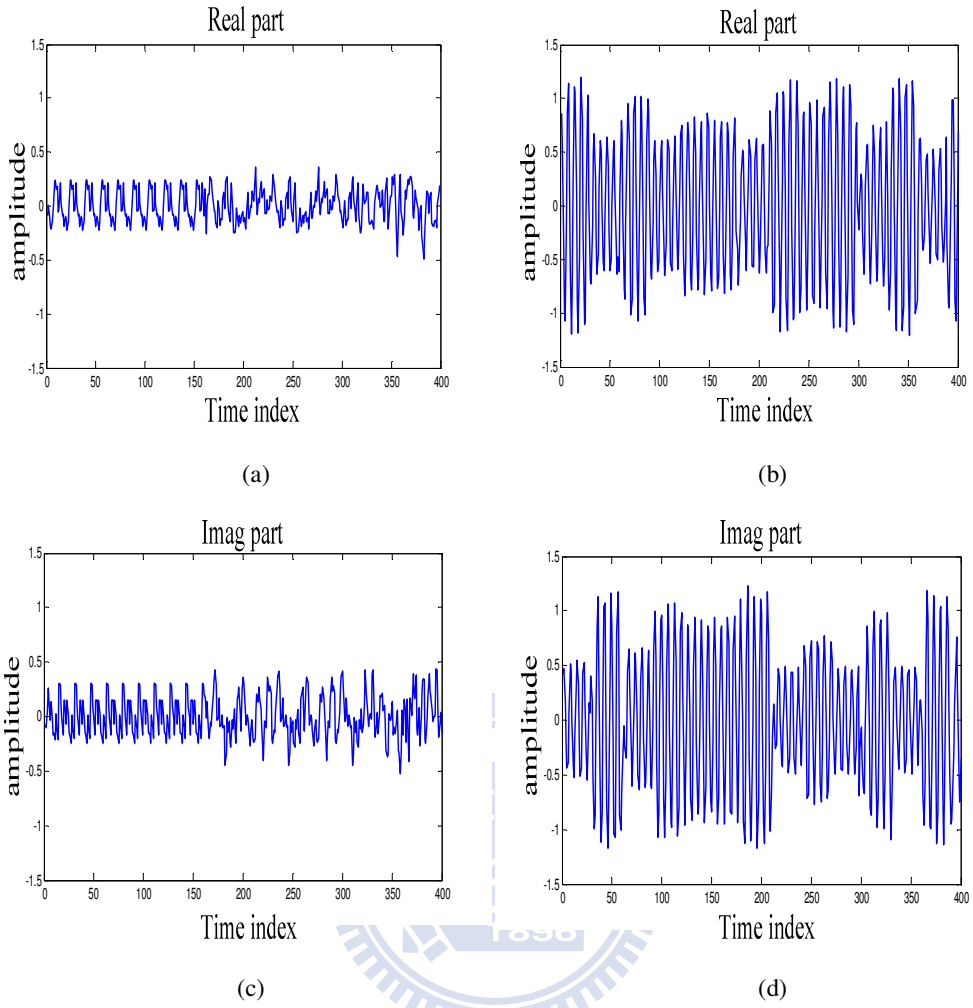

Figure 3-1 (a)The real part of preambles in time domain. (b)The real part of CW jamming in time domain. (c)The image part of preambles in time domain. (c)The image part of CW jamming in time domain.

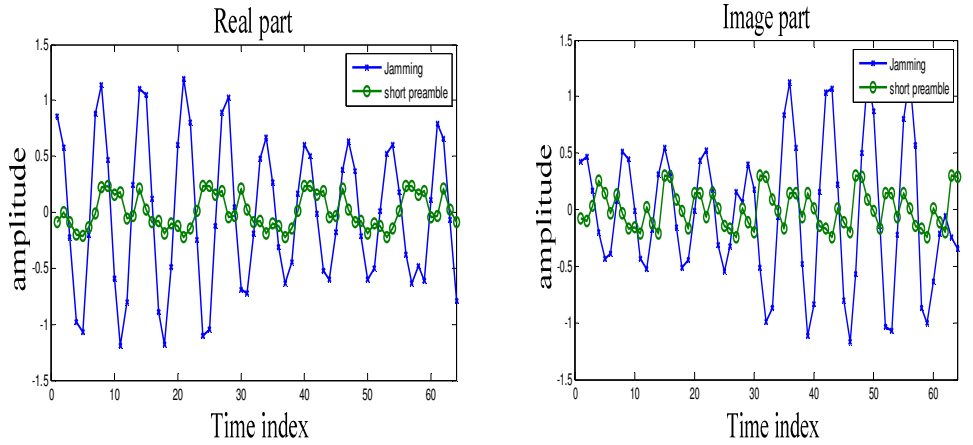

Figure 3-2 64 samples taken from preamble and CW jamming.

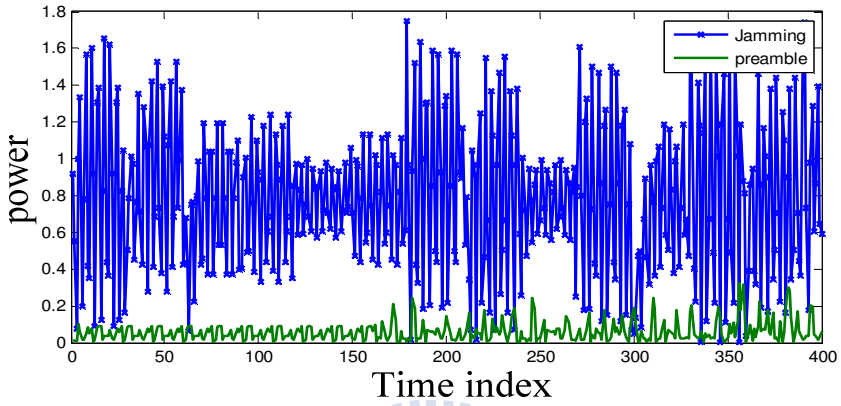

(a)

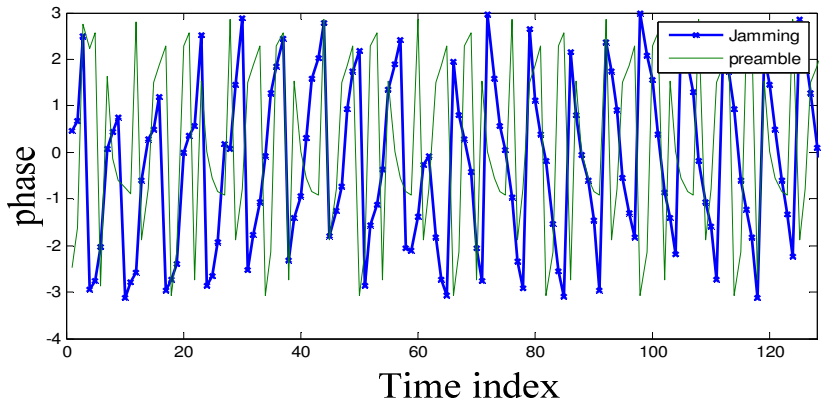

(b)

Figure 3-3 Power and phase of preambles and CW jamming in time domain.

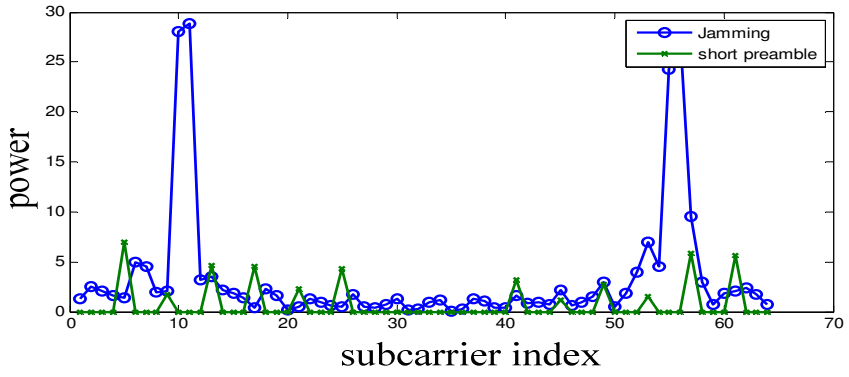

(a)

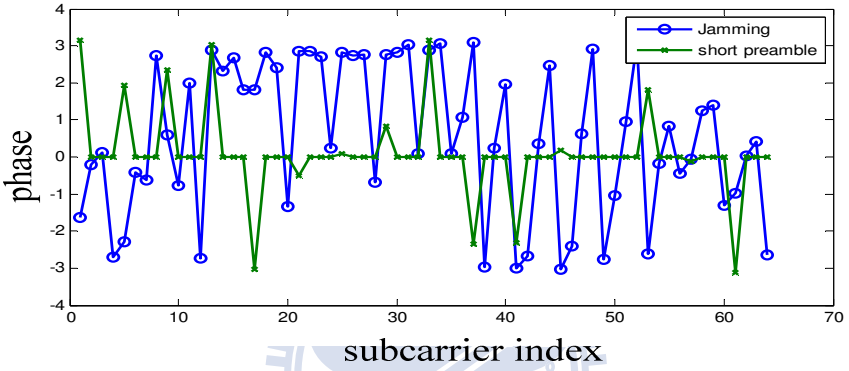

(b)

Figure 3-4 Power and phase of preambles and CW jamming in frequency domain.

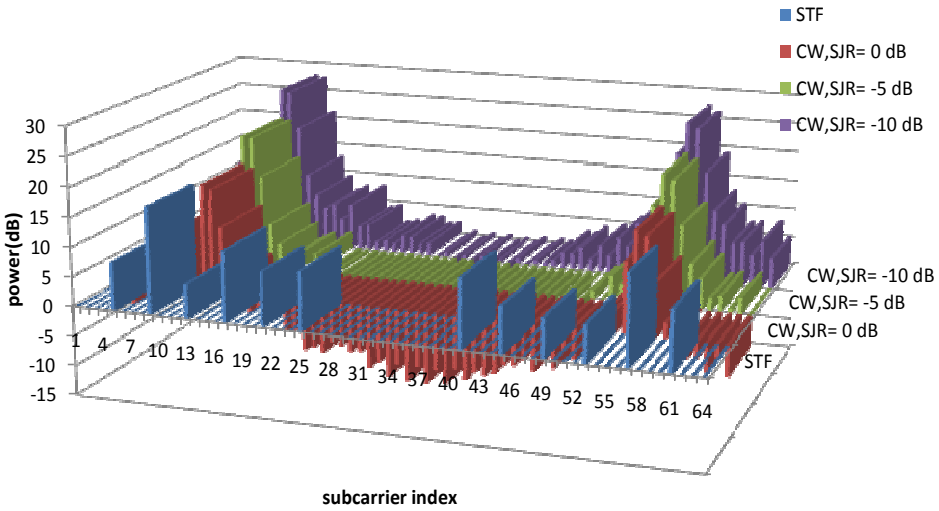

Figure 3-5 Power Distribution on Each Subcarrier Index.

3.2.2 Ratio of CW Jamming and Preamble Patterns in Aspect of Power

From figure 3-5, STF only has its value on 12 positions of subcarrier index. These 12 values are collected to calculate the ratio of CW jamming of short preamble. The statistics of figure 3-6 (a) is shown as power distribution on 12 positions. Compared with the ratio of index 4~9, he ratio of index 1~3 and index 10~12 is higher due to two peaks of CW jamming, as can be seen in figure 3-6 (b).

Even if the position suffered from less attack, the power of CW jamming on these positions still cannot be ignored when SJR=-10 dB. Under this circumstance, reducing the power may be the way to solve the effect of CW jamming.

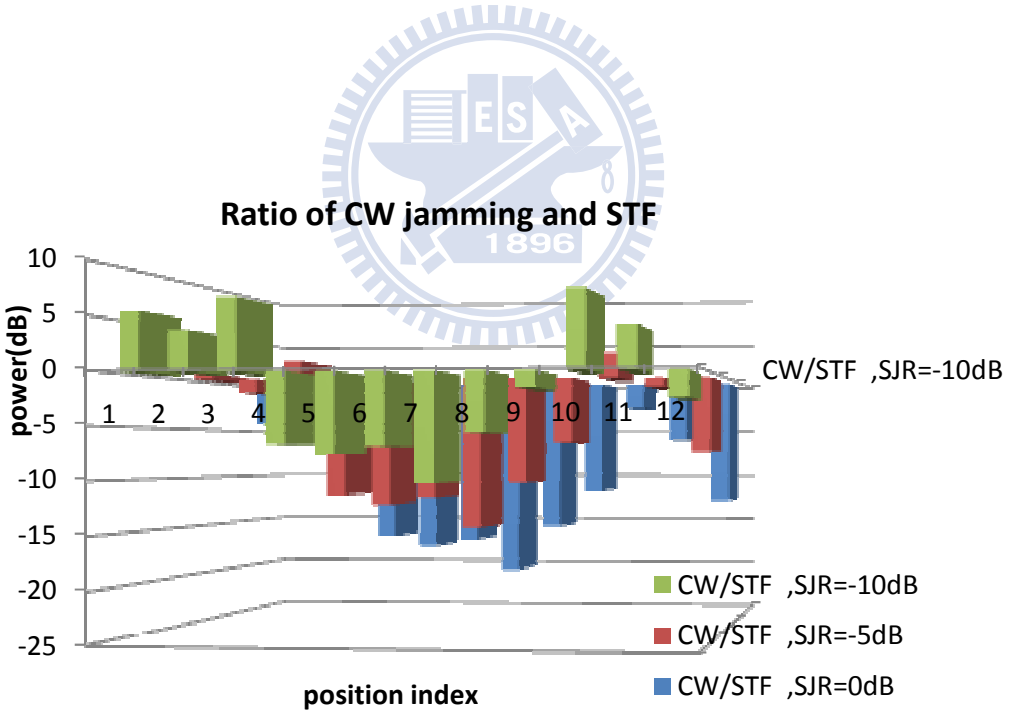

(a)

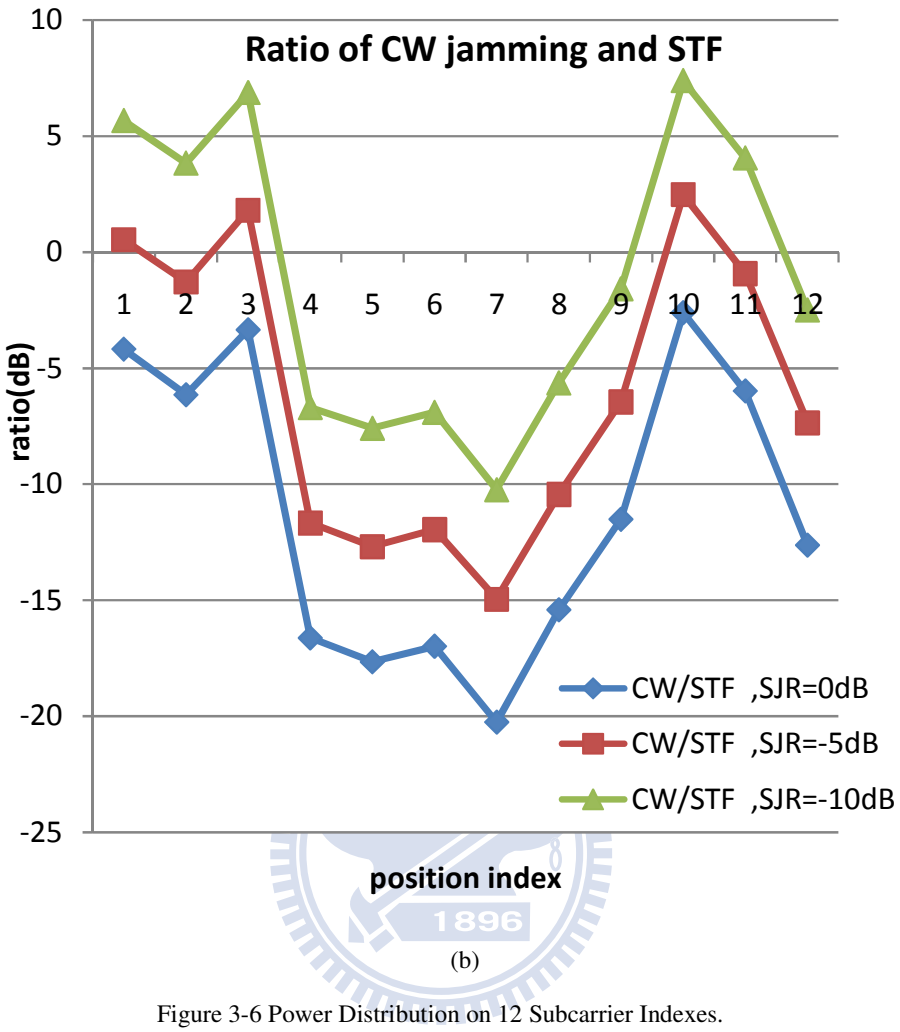

(b)

Figure 3-6 Power Distribution on 12 Subcarrier Indexes.

3.3 CW Jamming Detection

The desired signal is mixed with CW jamming over transmission. When the desired signal is received at receiver, it is actually hard to get the information about CW jamming, such as its amplitude, phase, carrier frequency, and power. However, some phenomenon is observed after taking CW jamming into FFT. The frequency spectrum of CW jamming will display two high peaks. If they exceed some threshold which is given by one reasonable value, CW jamming does interfere with the transmitted signal. Therefore, some methods for resisting CW jamming should be

turned on.

3.4 Anti-Jamming Method

When modulation of CW jamming is ASK or BPSK and CW jamming close to the receiver is assumed. The CW jamming is simplified as [21]:

$$i(t) = A \cdot \cos(2\pi ft + \theta), \tag{27}$$

where represents the amplitude of a jammer, f represents the carrier frequency of a jammer, θ represents the phase offset of a jammer. Because $i(t)$ is a real number, the Fast Fourier Transform (FFT) of $i(t)$ will meet this property:

$$I(N-k) = I^*(k). \tag{28}$$

where N is the point number of FFT, k is subcarrier index, and * means conjugate.

By using this property of conjugate symmetric (28) and digital signal processing, CW jamming can be cancelled totally and then has no effects on estimating IQ mismatch. The received signal can be written as:

$$R_1(k) = \alpha \hat{H}_{11}(k) L\text{-}STF_1(k) + \beta \hat{H}_{11}^*(-k) L\text{-}STF_1^*(-k) + (\alpha+\beta) I(k). \tag{29}$$

Equation (29) can be rewritten as

$$\frac{R_1(k)}{(\alpha+\beta)} = \frac{\alpha \hat{H}_{11}(k) L\text{-}STF_1(k) + \beta \hat{H}_{11}^*(-k) L\text{-}STF_1^*(-k)}{(\alpha+\beta)} + I(k). \tag{30}$$

And symmetric position of subcarrier index is used to cancel CW jamming, i.e. index k and index N-k, index k+1 and index N-k-1.

$$\begin{aligned} &\frac{R_1(k)}{(\alpha+\beta)} - \frac{R_1^*(N-k)}{(\alpha+\beta)} \\ &= \frac{\alpha \hat{H}_{11}(k) L\text{-}STF_1(k) + \beta \hat{H}_{11}^*(-k) L\text{-}STF_1^*(-k)}{(\alpha+\beta)} \\ &- \frac{\alpha^* \hat{H}_{11}^*(N-k) L\text{-}STF_1^*(N-k) + \beta \hat{H}_{11}^*(-N+k) L\text{-}STF_1^*(-N+k)}{(\alpha+\beta)^*}. \end{aligned} \tag{31}$$

Then the new equation (31) is rearranged and calculated to a new IQM

coefficient which will be used to estimate a new CFR. After that, these step last iteratively and an accurate IQ value will be obtained.

However, the modulation of information cannot usually be obtained and so the above method is impractical. By observing the behavior of CW jamming in frequency domain, the variation of CW jamming is not large between two training symbols is assumed. A new idea is proposed that short training field is subtracted from long training field after FFT. Expectedly, the influence on CW jamming could be mostly reduced.

3.5 Peak-Avoidance Method (PEAM)

From frequency spectrum view, the magnitude of the jamming displays two peaks on the positive subcarrier index and the corresponding negative subcarrier index. Figure 3-7 illustrates that legacy short training fields (L-STF) which are far away from the peak suffer from less power of the jamming. These L-STFs which are corrupted by less power are used to estimate IQ mismatch and theoretically should show more accurate estimated values. Furthermore, one estimated result is obtained from each STF. By making use of statistical techniques, mean and variance of these data are calculated. When data which have bigger variances are discarded and then the remainders are averaged, the estimated value is more correct. This concept can also apply to high-throughput short training fields (HT-STF).

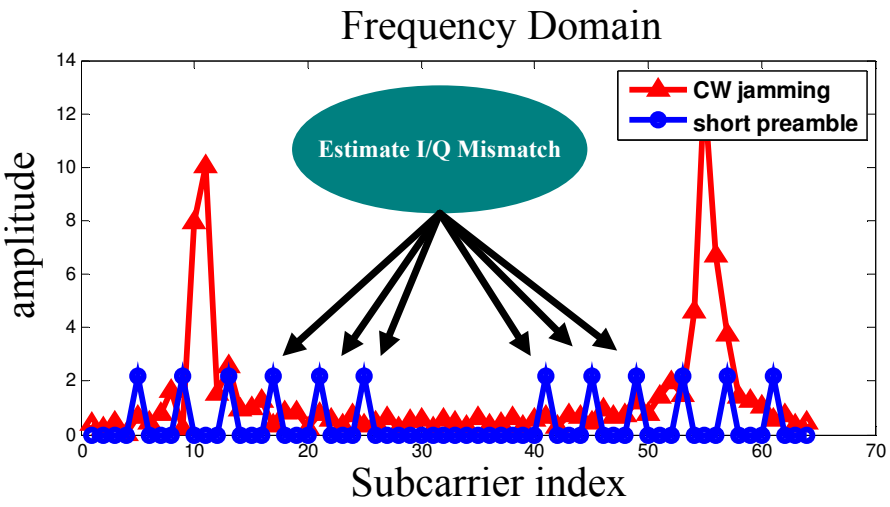

Figure 3-7 CW Jamming and L-STF in Frequency Domain.

3.6 Smooth Filter

Based on equation (25), multipath fading channels need to be estimated first to acquire a rough channel frequency response (CFR) in the frequency domain. However, the estimation of the CFR is destroyed totally by CW jamming and then the estimation of IQ mismatch becomes very inaccurate. Therefore, a smooth filter which has five taps is designed to lower the peak value of CFR. Figure 3-8 represents a block diagram of a smooth filter and its mathematical equation expressed as:

$$y[n] = \sum_{l=0}^{4} h[l] \cdot x[n-l], \tag{32}$$

where l represents the number of delay and $h[l]$ represents weight of the input.

Figure 3-9 illustrates that the magnitude of CFR becomes more approximate to the original channel through smooth filter, and although it is unequal to the original, it can make the estimation of IQ mismatch more correct.

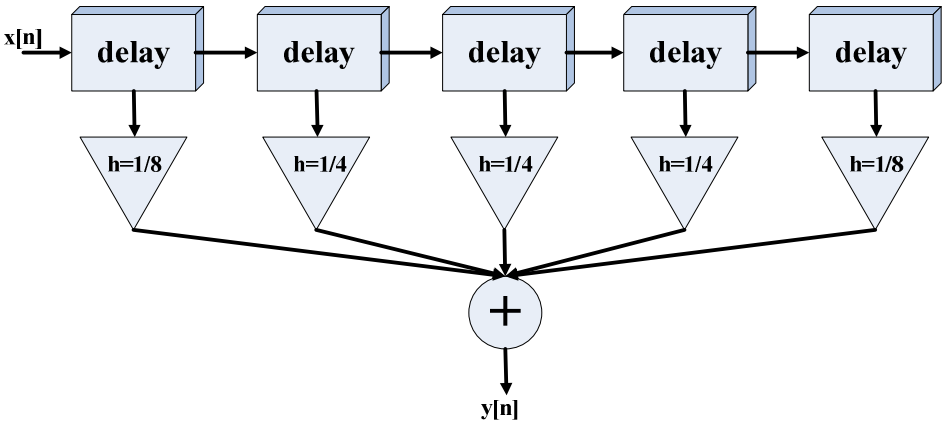

Figure 3-8 Smooth Filter block diagram.

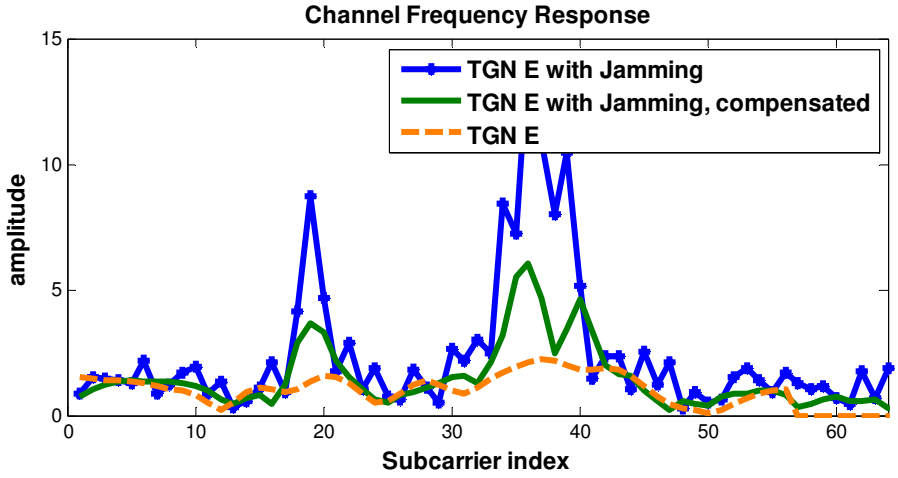

Figure 3-9 Channel Frequency Response.

3.7 Averaging Method in Time Domain (TD-AVM)

In this paper, the cyclic prefix (CP) length greater than the rms delay spread of multipath fading channel is assumed. And when the transmitted signal only suffers from AWGN, multipath fading channel and I/Q mismatch without being interfered with CW jamming, the received legacy short training (L-STF) and the high-throughput short training symbol (HT-STF) repeat every sixteen samples in time domain. By exploiting the periodicity of patterns, power of CW jamming can be reduced to obtain better IRR. The concept of averaging method is to average five L-STFs to get one new L-STF and then make three copies of this new one to form four L-STFs. Transforming four L-STFs from time domain into frequency domain by

FFT, the distribution of power of CW jamming is lower than before averaging. Therefore, a more precise IQM coefficient can be estimated.

The concept of this method is to make CW jamming become periodical signal in one FFT interval without changing short preamble at the same time. When SJR=-10dB and 1000 packets are used to get a statistics. Figure 3-10 shows that power of CW jamming on each subcarrier index declines after TD-AM, excluding the index which two peaks occupy. From statistical view, index 17 is taken for example; after TD-AM, its probability density function (PDF) moves left, as can be seen from figure 3-11. Moving left presents that the averaging power of CW jamming is reduced by TD-AVM.

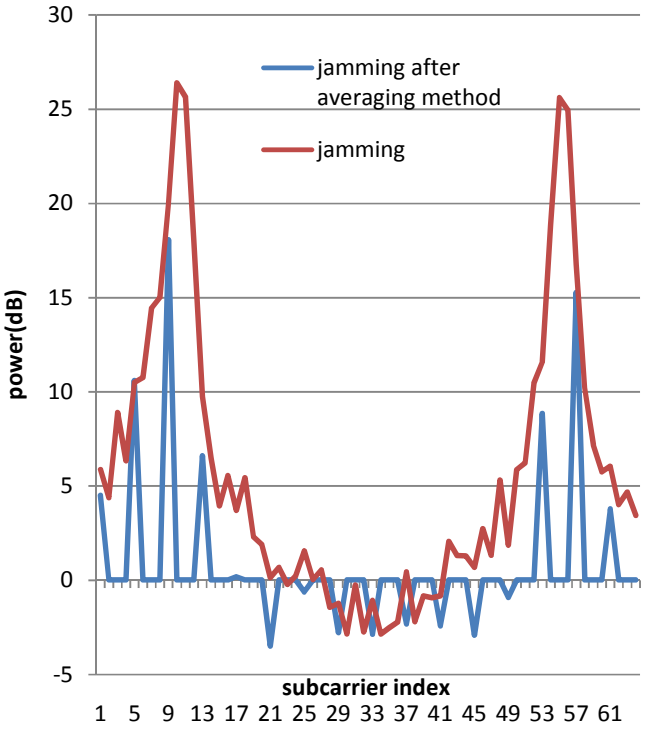

Figure 3-10 Comparison of power of CW jamming between before and after TD-AVM.

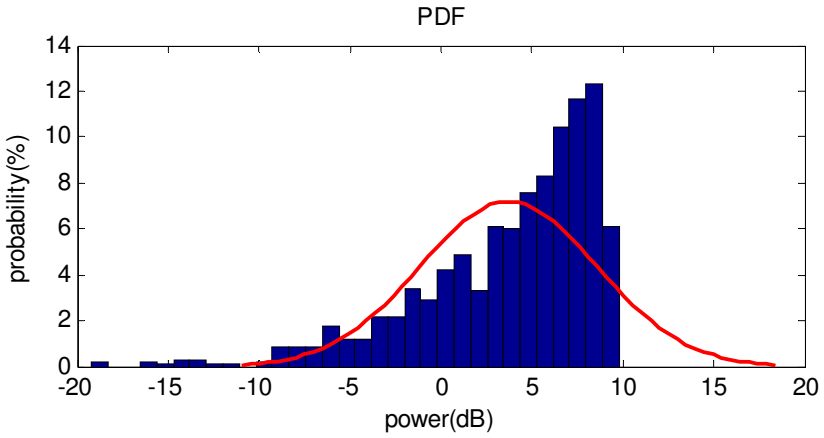

(a)

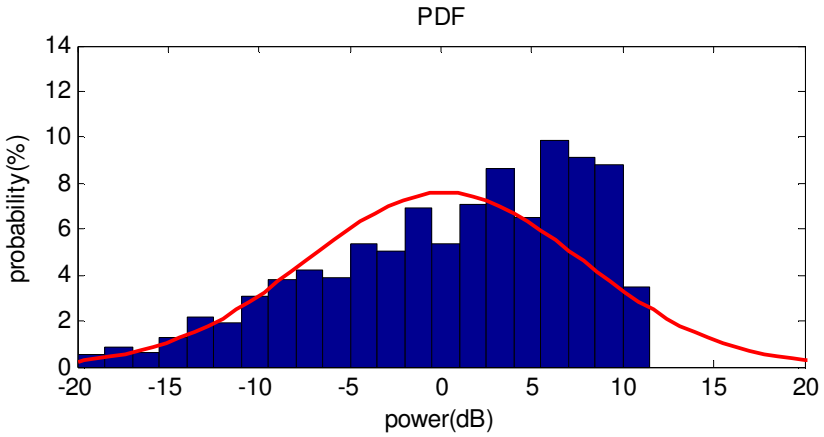

(b)

Figure 3-11Probability density function (PDF) of power of Subcarrier index 17. (a)Before TD-AVM. (b)After TD-AVM.

3.8 The Proposed Algorithm of I/Q Estimation with CW Jamming

The proposed algorithm can be summarized as follows:

1) Detect whether CW jamming exist or not. If not, execute the FD-IQME algorithm described in section 3.1; otherwise, go to 2).

2) Use smooth filter to improve the estimation of a rough CFR.

3) Execute the averaging method (TD-AVM) described in section 3.7.

4) After FFT, perform the FD-IQME algorithm and then the peak-avoidance

method (PEAM) described in section 3.5.

Figure 3-12 shows the proposed algorithm structure in the receiver; Figure 3-13 shows the flow char of the proposed algorithm.

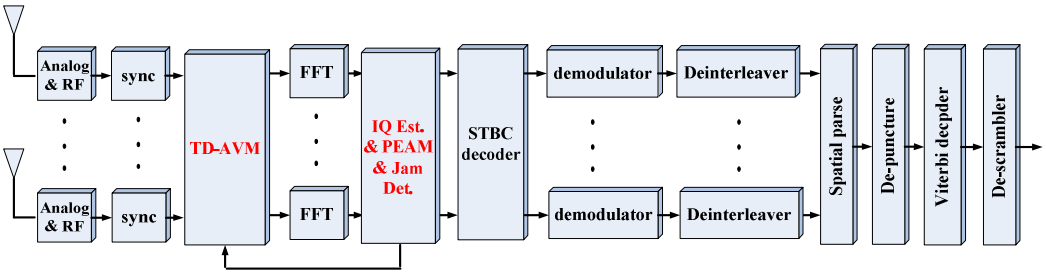

Figure 3-12 The proposed algorithm structure in Rx.

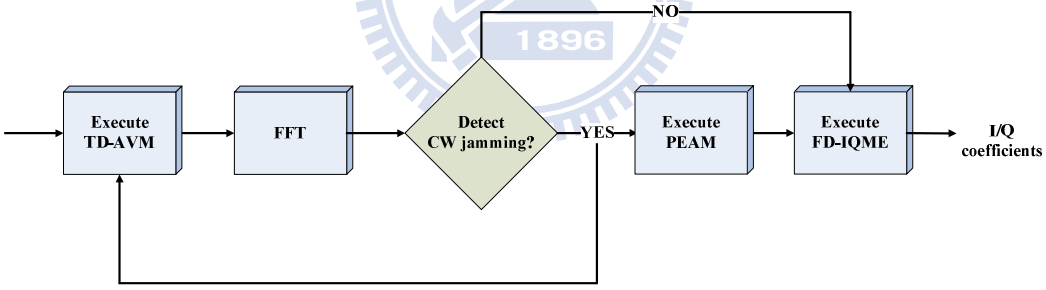

Figure 3-13 The flow chart of the proposed algorithm.

Chapter 4

Simulation Results and Performance

4.1 Simulation Results of Only I/Q-Mismatch

A typical MIMO-OFDM system with FD-IQME algorithm is simulated to evaluate and compare the performance. The length of OFDM symbol is 64 samples and cyclic prefix is 16 samples. The parameters used in the simulation are as follows:

- 4X4 MIMO-OFDM systems in 20 MHz.
- PSDU is 1024 bytes
- 1000 packets
- Multipath Mode: TGn E.
- Modulation:64 QAM, coding rate:2/3
- SJR=-10dB each receiver
- I/Q Mismatch :

  gain error :1dB, phase error:20° in receiver one

  gain error :2dB, phase error:13° in receiver two

  gain error :2dB, phase error:18° in receiver three

  gain error :1dB, phase error:19° in receiver four

Figure 4-1 shows that the performance of FD-IQME algorithm is acceptable.

Without CW jamming, packet error rate (PER) converges to 0.01 as signal-to-noise ratio (SNR) equals to 20 dB; bit error rate (PER) declines to 10^{-5} as signal-to-noise ratio (SNR) equals to 20 dB.

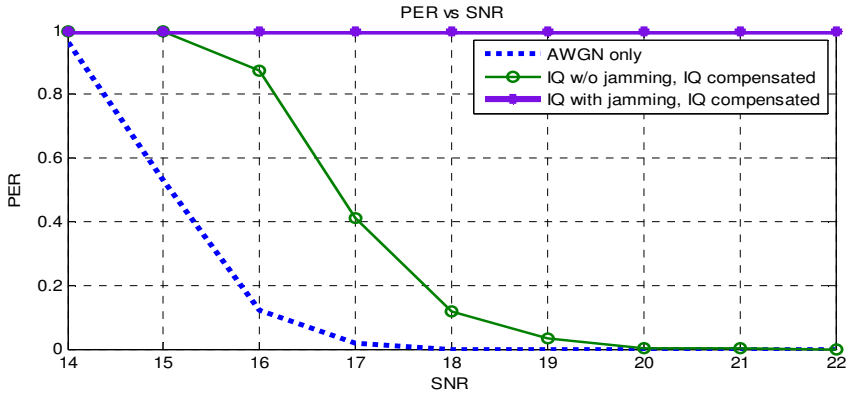

(a)

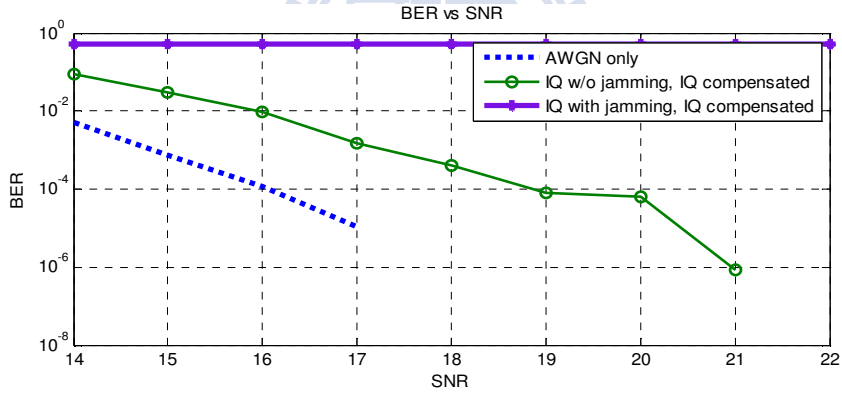

(b)

Figure 4-1 The Compensation Result.

4.2 Performance Index

The aim of this paper is to estimate IQM coefficients correctly under the attack of CW jamming. Accurate IQM coefficients, which are obtained from FD-IQME once, can be used to compute CFR again and compensate data. Due to huge simulation time, the system performance is based on the image rejection ratio (IRR). The image rejection ratio as a function of the mismatch is denoted as [22]:

$$\begin{aligned} IRR(dB) &= 10 \cdot \log_{10} \frac{desired\ signal}{image\ signal} \\ &= 10 \cdot \log_{10} \frac{1+(1+\Delta\varepsilon)^2 + 2\cdot(1+\Delta\varepsilon)\cdot\cos\Delta\theta}{1+(1+\Delta\varepsilon)^2 - 2\cdot(1+\Delta\varepsilon)\cdot\cos\Delta\theta}, \end{aligned} \tag{33}$$

where $\Delta\varepsilon = \left|\varepsilon - \hat{\varepsilon}\right|$ represents the difference of the gain error along the I and Q signal paths, while $\Delta\theta = \left|\theta - \hat{\theta}\right|$ represents the difference of the deviation of the local oscillators from quadrature. From figure 4-2, no I/Q mismatch means that IRR approximates 49 dB when $\Delta\varepsilon = 0$ *and* $\Delta\theta = 0$. In other words, the higher IRR value presents accurate estimations.

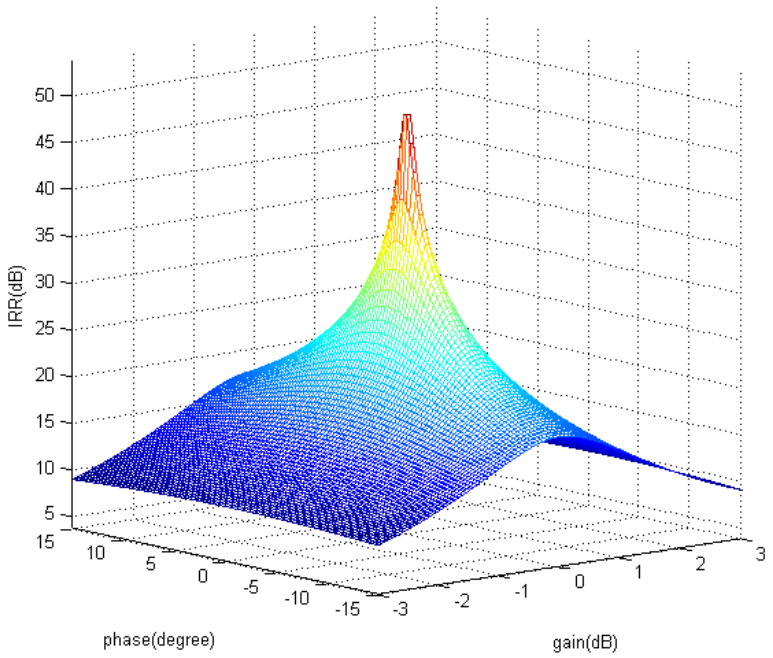

Figure 4-2 IRR values corresponding to different phases and gains.

4.3 Simulation Results of I/Q-Mismatch with CW Jamming

For convenience of representation, the abbreviation is used for the proposed methods as below.

- FD-IQME : I/Q-Mismatch Estimation in Frequency Domain.
- SF : Smooth filter.
- SP-LP : Short preamble subtracted from long preamble.
- PEAM : Peak-Avoidance Method.
- TD-AVM : Averaging Method in Time Domain.

The estimated IQM coefficients on Receiver one is taken to analyze the performance of each method. Because PER and BER converge on SNR=20dB, SNR will be fixed on 20dB when these proposed methods above are discussed. And SJR=-10dB.

4.3.1 Evaluate FD-IQME

While FD-IQME is used to estimate IQM coefficients without dealing with CW jamming, IRR approximates 12 dB from Table 4-1. However, IRR approximates 36 dB when there is no CW jamming. The gap is about 24 dB, which means that CW jamming must be considered when estimating IQM coefficients; this result can correspond to Figure 4-1.

Actually, the IRR value, which is calculated, is only a point. However, it is convenient to observe so that the point is expanded to one plane; the yellow plane is expanded form the point of 35.96 dB and the green plane is expanded form the point of 11.93 dB, as can be seen from Figure 4-3.

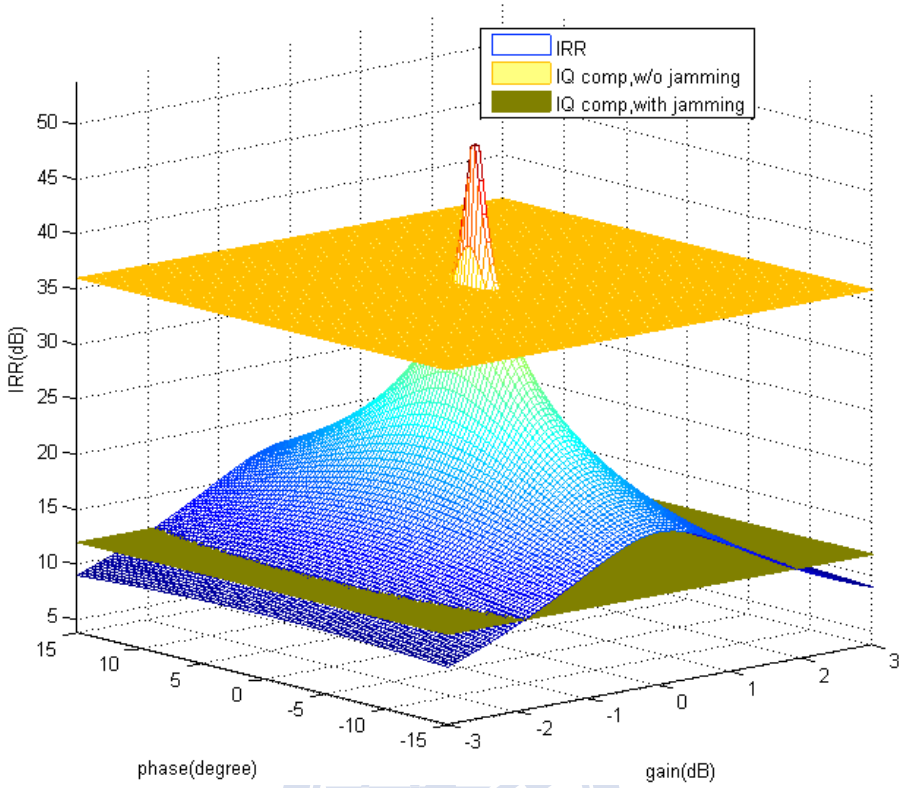

Figure 4-3 IRR, comparison of FD-IQME w/o jamming and FD-IQME with CW jamming.

Table 4-1 IRR, comparison of FD-IQME w/o jamming and FD-IQME with CW jamming.

FD_IQME	***Δ ε (dB)***	***Δ θ (degree)***	***IRR (dB)***
w/o jamming	0.032	0.798	**35.96**
With jamming	1.046	22.972	**11.93**

4.3.2 Evaluate SF & SP-LP

From Figure 4-4, using smooth filter, which makes IRR reduced to 9 dB, is worse than using no smooth filter. The result shows that this method SF is not robust enough. The main reason is that smooth filter does not assure that the estimated CFR can approximate the real CFR but rather that the two peak which are caused by CW jamming can be suppressed. Nevertheless, the estimated CFR, which is adjusted by the smooth filter, is still not available, even worse.

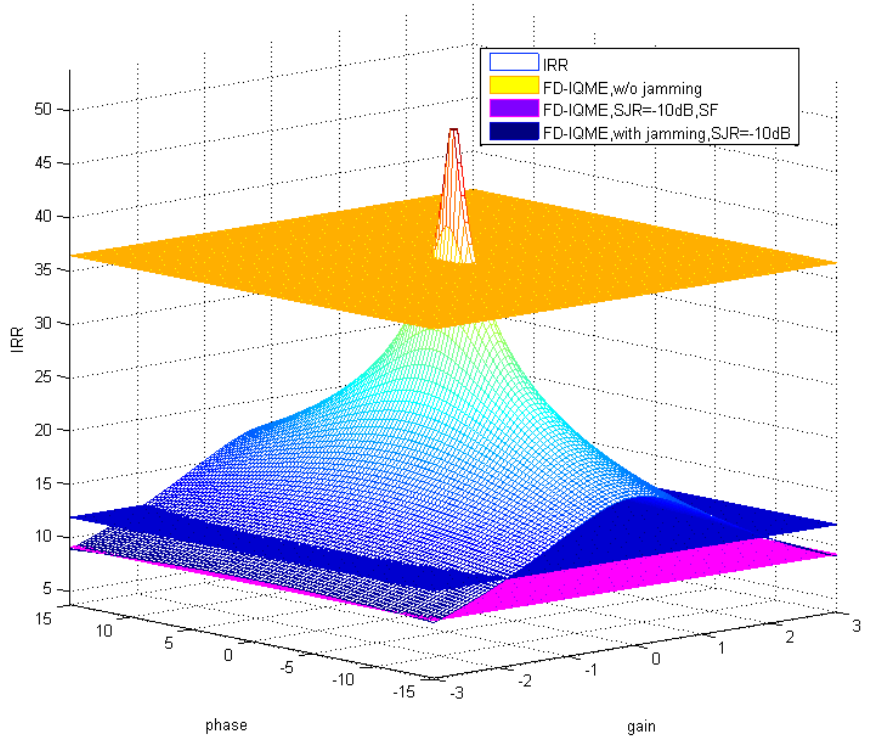

Figure 4-4 IRR, comparison of FD-IQME w/o jamming, FD-IQME with CW jamming, and FD-IQME+SF with jamming.

When SP-LP is evaluated, the ideal CFR is assumed. From Figure 4-5, using the method SP-LP makes IRR reduced to 6.5 dB, compared to using no methods. This purpose of SP-LP is to use two adjacent preambles to cancel CW jamming. However, this does not work because CW jamming is time variant and changes according to

changing rate (CR). Two adjacent CW jammings are always different, which makes SP-LP fail to eliminate CW jamming.

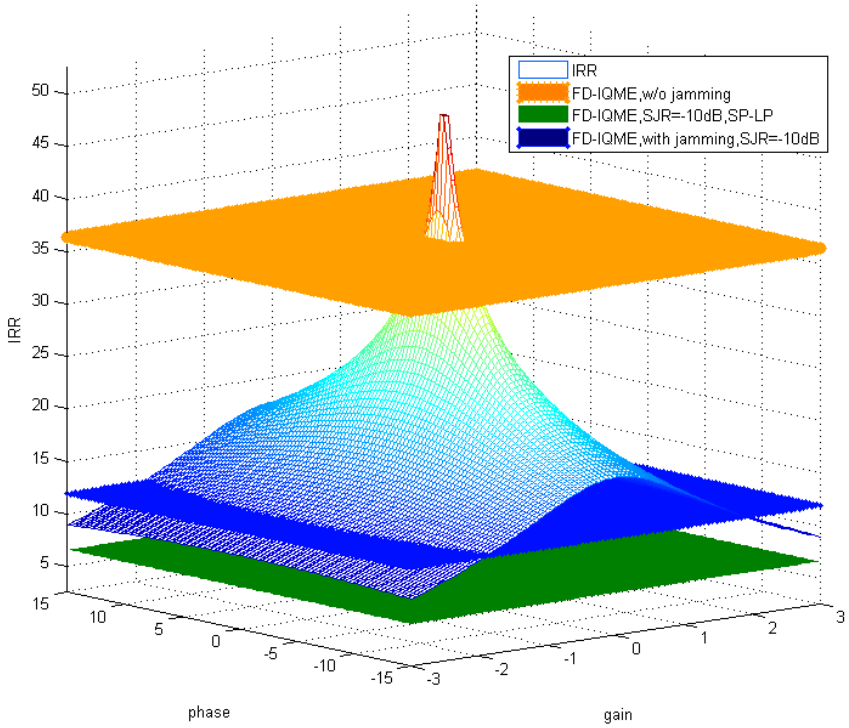

Figure 4-5 IRR, comparison of FD-IQME w/o jamming, FD-IQME with CW jamming, and FD-IQME+SP-LP with jamming.

4.3.3 Evaluate PEAM & TD-AVM

Because I/Q-Mismatch estimation needs the information of CFR to calculate IQM coefficients, those simulations in this section are based on knowing the ideal CFR, which is not corrupted by CW jamming. The simulation results are based on 1000 packets. From Figure 4-6 and Table 4-2, some observations are obtained. Using PEAM and FD-IQME can get 19.16dB of IRR, which is better than 11.96dB while using only FD-IQME. If TD-AVM, PEAM and FD-IQME are used for estimating IQM coefficients, IRR will increase into 22.25dB. This justifies that the power of CW jamming is reduced mostly. Figure 4-6 clearly shows that the mean value of IRR moves from 11.96dB to 22.25dB.

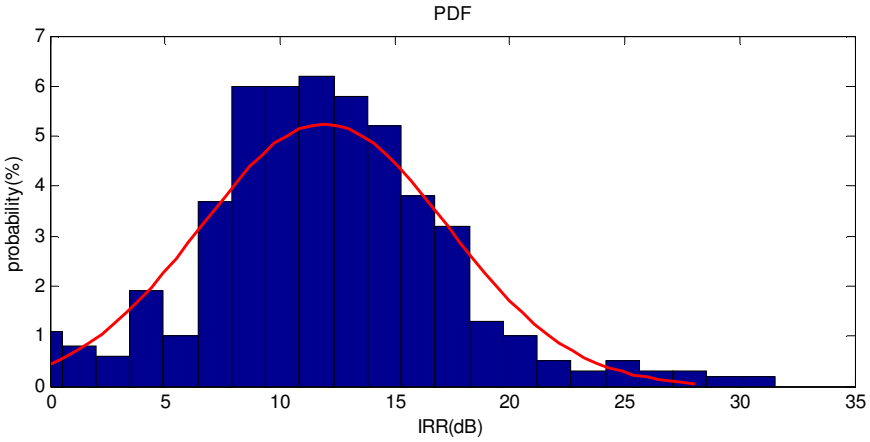

(a)

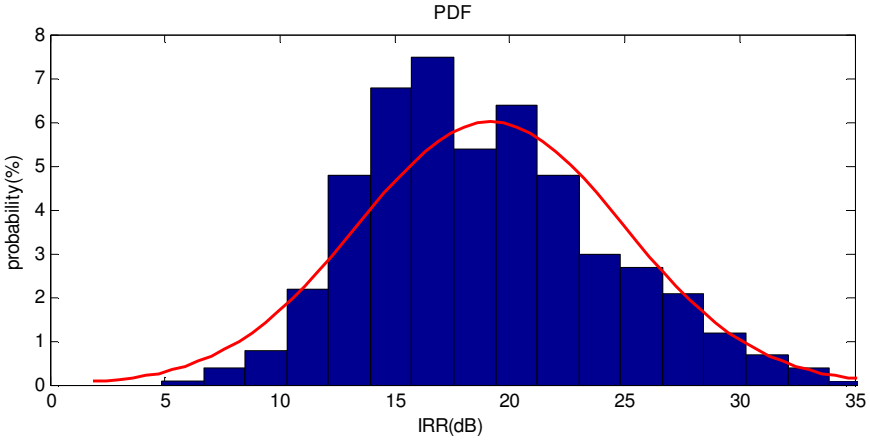

(b)

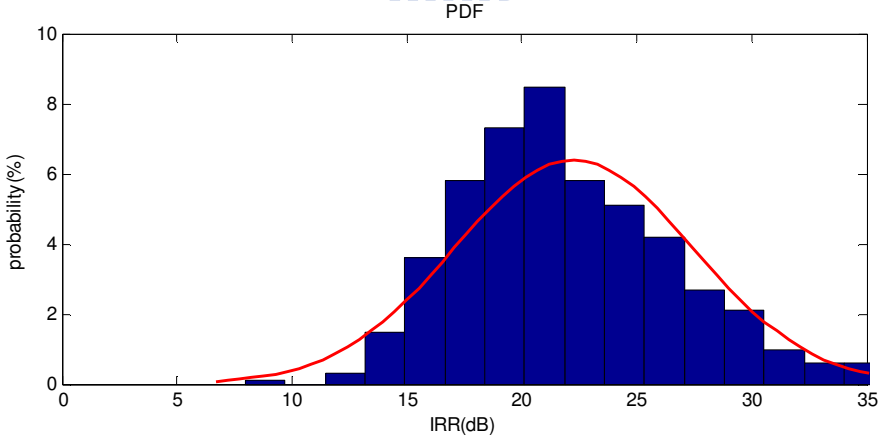

(c)

Figure 4-6 Probability density function (PDF) of IRR. (a) FD-IQME.

(b) PEAM+ FD-IQME.(c) TD-AVM+PEAM+ FD-IQME

Table 4-2 IRR, comparison of FD-IQME, PEAM+ FD-IQME, and TD-AVM+PEAM+ FD-IQME.

with jamming	$\Delta\varepsilon$ *(dB)*	$\Delta\theta$ *(degree)*	*IRR (dB)*
TD-AVM + PEAM + FD-IQME	0.130	6.575	**22.25**
PEAM + FD-IQME	0.203	9.321	**19.16**
FD-IQME	1.046	22.972	**11.93**

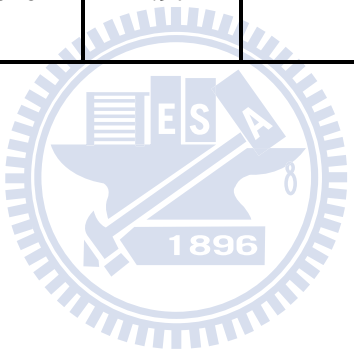

4.3.4 Brief Summary

From Figure 4-7 and Table 4-3, by using the proposed methods, FD-IQME, PEAM, the performance can increase to 19.16dB; by using the proposed methods, FD-IQME, PEAM and TD-AVM, the performance can increase to 22.25dB. Compared with using only FD-IQME, about 10 dB of improvement is obtained. In the future, some digital signal processing (DSP) techniques such as linear regression can be used to reach higher IRR .

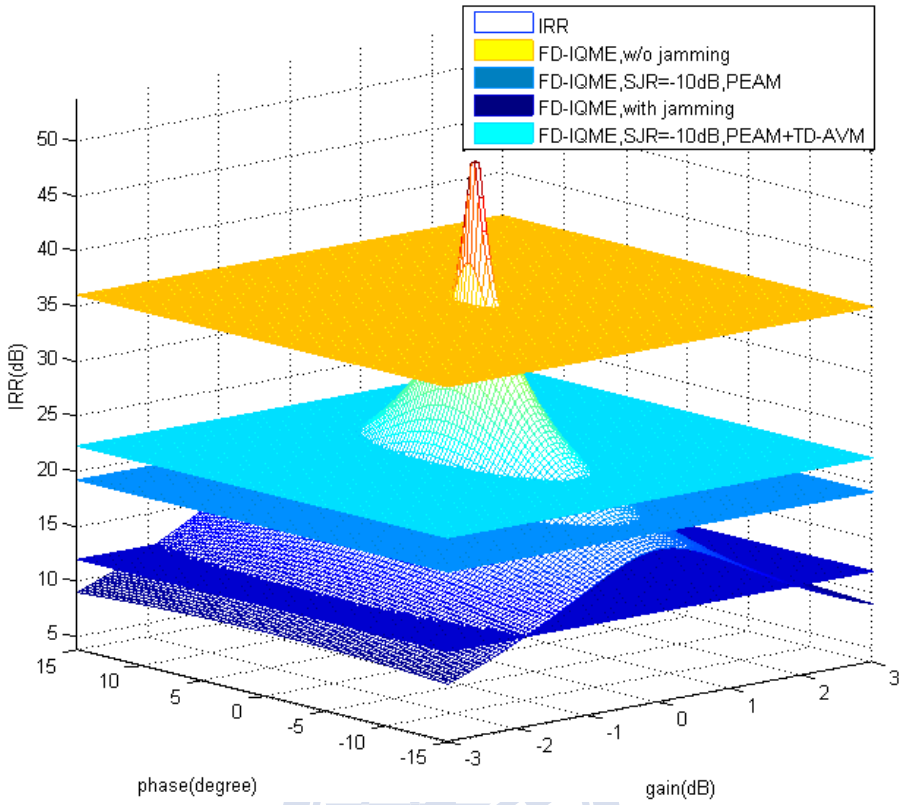

Figure 4-7 IRR, comparison of FD-IQME w/o jamming, FD-IQME with jamming, PEAM+ FD-IQME with jamming, and TD-AVM+PEAM+ FD-IQME with jamming.

Table 4-3 IRR, comparison of FD-IQME w/o jamming, FD-IQME with jamming, PEAM+ FD-IQME with jamming, and TD-AVM+PEAM+ FD-IQME with jamming.

Methods	***FD-IQME***	***PEAM***	***TD-AVM***	***IRR (dB)***
w/o CW Jamming	√			**35.96**
With CW Jamming	√			**11.93**
	√	√		**19.16**
	√	√	√	**22.25**

Chapter 5

Conclusions and Future Work

5.1 Conclusions

The currently existing methods which are evaluated seem to provide some resistance to CW jamming. However, a robust method for solving CW jamming is needed. Therefore, time-domain estimator for IQ mismatch with CW jamming is considered to evaluate. As mentioned in the Section 3, while the power of CW jamming is reduced once, the IRR will improve significantly. The proposed methods and the simulation results demonstrate this idea. This concept also can be applied to the time-domain estimator.

The main contribution for this paper is as follows. First, by making use of STF, one shot calculated algorithm is proposed to estimate IQM coefficients without too complicated computations. Second, by defining image-rejection-ratio (IRR), the simulation time can be effectively reduced to obtain estimated IQM coefficients.

5.2 Future Work

In this section, three works are suggested to solve in the future. First, a I/Q mismatch estimation in time domain is proposed to resist CW jamming. Second, a

accurate channel-estimation is needed. Finally, the hardware implementation is continued.

5.2.1 I/Q Mismatch Estimation in Time Domain

From time domain view, the amplitude of CW jamming covers the one of desired signal due to SJR equal to -10 dB. By reducing the power of CW jamming, the performance of estimating IQ mismatch will improve greatly. Some property of STF can be used to reduce the power of CW jamming. For many positions of STF are null subcarriers in the frequency domain. If CW jamming corrupted the signal, the values of these positions will become nonzero. However, these values are forced to set to ZERO and that will not destroy the original signal because the values of these positions do not include the values of the original transmitted signal. And then the results are transformed from frequency domain to time domain by IFFT. After that, the power of CW jamming is reduced mostly and makes little effects on the signal. But this method needs a time-domain estimator for I/Q mismatch.

5.2.2 Channel Estimation

Although a smooth filter is used to resist CW jamming, the performance of IRR is not good enough. For I/Q estimation in frequency domain, the estimation of channel frequency response (CFR) also affects the estimation of IQM coefficients. If a rough value of estimated CFR cannot be compensated, IRR is always very low. Therefore, an anti-jamming channel-estimation is needed.

5.2.3 Hardware Implementation

The FD-IQME algorithm of 4X4 MIMO-OFDM system will be performed by verilog and then tap out. Therefore, RTL coed, gate-level verification, and layout need to be completed in the future.

Bibliography

[1] A. Tarighat, E. Bahheri, and A. H. Sayed, “Compensation schemes and performance analysis of IQ imbalances in OFDM receivers,” IEEE Trans. Signal Process., Aug. 2005.

[2] M. Valkama , M. Renfors, and V. Koivunen, “Compensation of frequency-selective IQ imbalances in wideband receivers models and algorithms”, Wireless Communications, 2001. (SPAWC '01). 2001 IEEE Third Workshop on Signal Processing Advances in 20-23 March 2001 Page(s):42 – 45

[3] K.P. Pun, J.E. Franca, C. Azeredo-Leme, C.F. Chan,C.S. Choy, “Correction of frequency-dependent I/Q mismatches in quadrature receivers,” IEEE Electronics Letters, Volume 37, Issue 23, Page(s):1415–1417, Nov 2001.

[4] P. Rykaczewski, J. Brakensiek, F.K. Jondral, “Decision directed methods of I/Q imbalance compensation in OFDM systems,” IEEE 60th Vehicular Technology Conference (VTC2004-Fall), Volume 1, Page(s):484-487, Sept. 2004.

[5] M. Valkama, M. Renfors, V. Koivunen, “Advanced methods for I/Q imbalance compensation in communication receivers” IEEE Transactions Signal Processing, Volume 49, Issue 10, Page(s):2335–2344, Oct. 2001.

[6] J. Tubbax, A. Fort, L. Van der perre, S. Donnay, M. Engels, H. De Man, “Joint compensation of IQ imbalance and frequency offset in OFDM systems,“ in Proc. GLOBECOM, vol. 4, pp.2365-2369, Dec 1-5. 2003

[7] P. Zhang, T. Nguyen, C. Lam, D. Gambetta, T. Soorapanth, B. Cheng, S. Hart, I. Sever, T. Bourdi, A. Thaam, and B. Razavi, “A 5-GHz direct-conversion CMOS transceiver,” Solid-State Circuits, IEEE Journal of , vol.38, no.12, pp. 2232-2238, Dec. 2003

[8] D. Gerakoulis and P. Salmi, “An interference suppressing OFDM system for wireless communication,” in IEEE International Conference on Communications (ICC), New York, NY, Apr. 2002, pp. 480–484.

[9] Z. Wu and C. R. Nassar, “Narrowband interference rejection in OFDM via carrier interferometry spreading codes,” IEEE Trans. Wireless Commun., vol. 4, pp.1491–1505, July 2005.

[10] G. Carron, R. Ness, L. Deneire, L. V. der Perre, and M. Engles, “Comparison of two modulation techniques using frequency domain processing for in-house networks,” IEEE Trans. Consumer Electron., vol. 47, pp. 63–72, Feb. 2001.

[11] R. Nilsson, F. Sj¨oberg, and J. P. LeBlanc, “A rank-reduced LMMSE canceller for narrowband interference suppression in OFDM-based systems,” IEEE Trans. Commun., vol. 51, pp. 2126–2140, Dec. 2003.

[12] D. Darsena, “Successive narrowband interference cancellation for OFDM systems,” IEEE Commun. Lett., vol. 11, pp. 73–75, Jan. 2007.

[13] A. J. Redfern, “Receiver window design for multicarrier communication systems,” IEEE J. Select. Areas Commun., vol. 20, pp.1029–1036, June 2002.

[14] A. J. Coulson, “Bit error rate performance of OFDM in narrowband interference with excision filtering,” IEEE Trans. Wireless Commun., vol. 5, pp. 2484–2492, Sept. 2006.

[15] Wireless LAN Medium Access Control (MAC) and Physical Layer (PHY) Specifications, IEEE Std 802.11a, 1999

[16] Ta-Yang Juan, “The Study of Pilot-based Adaptive Equalization for Wireless MIMO-OFDM Baseband Designs”, NCTU thesis, 2006

[17] Kan-Si Lin, “The study of Adaptive Equalization in MIMO-OFDM systems”, NCTU thesis, 2007

[18] January 2005.B. Cutler, “Effects of physical layer impairments on OFDM systems,” RF Design Magazine, May 2002.

[19] M. Valkama, and M. Renfors. “Advanced DSP for I/Q imbalance compensation in a low-IF receiver,” in Proc. IEEE Int. Conf. on Communications, New Orleans, LA,USA, Jun.2000.pp.768-772.

[20] M. Valkama , M. Renfors, and V. Koivunen,,.”Blind source separation based I/Q imbalance compensation,” in Proc. IEEE Symposium 2000 on Adaptive Systems for Signal Processing, Communications and Control, Lake Louise, Alberta, Canada, Oct. 2000, pp 310-314.

[21] Hsu-Feng Hsiao; Meng-Han Hsieh; Che-Ho Wei, "Narrow-band interference rejection in OFDM-CDMA transmission system ," Circuits and Systems, 1998. ISCAS '98. Proceedings of the 1998 IEEE International Symposium on , vol.4, no., pp.437-440 vol.4, 31 May-3 Jun 1998

[22] Rudell, J.C.; Ou, J.-J.; Cho, T.B.; Chien, G.; Brianti, F.; Weldon, J.A.; Gray, P.R., "A 1.9-GHz wide-band IF double conversion CMOS receiver for cordless telephone applications," Solid-State Circuits, IEEE Journal of , vol.32, no.12,

pp.2071-2088, Dec 1997